Winkler Model for Predicting the Dynamic Response of Caisson Foundations

S. Carbonari[1], Jacob D. R. Bordón[2*], Luis A. Padrón[2], M. Morici[3], F. Dezi[4], Juan J. Aznárez[2], G. Leoni[3], O. Maeso[2]

[1] DICEA, Università Politecnica delle Marche, Ancona, Italy

[2] ULPGC, Universidad de Las Palmas de Gran Canaria, Las Palmas de Gran Canaria, Spain

[3] SAAD, University of Camerino, Camerino, Italy

[4] SST, Geology Division, University of Camerino, Camerino, Italy

This is the pre-print version of the peer-reviewed manuscript of the following article: S. Carbonari et al, Winkler Model for Predicting the Dynamic Response of Caisson Foundations, Earthquake Engineering and Structural Dynamics (2022) which has been published in final form at: http://doi.org/10.1002/eqe.3713

Abstract.

The paper presents a Winkler-based numerical model for the analysis of the dynamic response of caisson foundations. The model allows the evaluation of the impedance functions and of the foundation input motion, which can be used in the framework of the substructure approach to compute inertial soil-foundation superstructure interaction analyses. In addition, kinematic stress resultants due to seismic shear waves propagating into the soil can be estimated. The caisson is modelled as a Timoshenko beam and the soil-caisson interaction forces are derived from the analyses of the plane-strain vibration problem of an annular rigid ring embedded into the soil. The problem solution is obtained in the frequency domain exploiting the finite element approach and generic soil stratigraphies can be considered in the applications. The model, which is characterised by a very low computational effort, is validated by performing a parametric investigation, comparing results with those obtained from more rigorous BEM-FEM models of the soil-caissons systems. Finally, some applications to real caisson foundations of offshore wind turbines are shown to demonstrate the model accuracy in capturing the seismic response of the foundations obtained from more rigorous models.

1 INTRODUCTION

A caisson foundation is a large, prefabricated box-type structure that can be sunk in soft grounds or water up to the required level by excavating or dredging the material within the caisson. The latter are similar in form to pile foundations but of greater diameters and smaller length-to-diameter ratios compared to piles, and can be classified depending on the installation technique. By excluding floating caissons, which are not embedded into the soil and are not of interest for this research, the following main typologies can be identified: open caissons, pneumatic caissons, suction caissons, and drilled pier. Open caissons are constituted by hollow shafts (chambers) with cutting edges, opened at both the top and the base, that sink into place by removing the soil from inside the shaft. If the soil within the shaft cannot be excavated easily or if water is expected to be a problem by filling in the excavated soil, pneumatic caissons can be employed; the latter are watertight box or cylinder-like structures opened at the bottom but closed at the top. In this case, compressed air is used to prevent the entry of water into the working chamber during the excavation. If the installation of the caisson foundation is offshore, a suction caisson may be preferrable. A suction caisson is an inverted bucket that is embedded in the marine sediment by creating a negative pressure inside the caisson skirt by pumping water out of the caisson; this technology is adopted when gravity loads are not sufficient for sinking the foundation into the ground and is particularly efficient for seabed with soft clays or low strength sediments. Finally, caissons may also be obtained by drilling a cylindrical hole of the desired depth in the soil and by filling it with concrete; in this case, the foundation is also known as drilled pier, and it can be characterised by a straight shaft or by a base enlargement.

The above foundation typologies have proved to be an extremely versatile solutions, able to withstand compressive, tensile or lateral loading, and are often adopted in both bridge and offshore engineering. In particular, caisson foundations can be used for bridge piers when high lateral forces and bending moments have to be faced, or when foundations are located below the water surface of rivers. In offshore engineering, caisson foundations are largely used for Offshore Wind Turbines (OWTs), for which the selection of the foundation typology is determined by the water depth [1]. Anyway, the previous structural typologies are both sensitive to the Soil-Structure Interaction (SSI) problem, which may largely affect

* Corresponding author: Jacob D. R. Bordón. ULPGC, Universidad de Las Palmas de Gran Canaria, jacobdavid.rodriguezbordon@ulpgc.es

their structural response when subjected to both seismic and non-seismic actions. As for bridges, SSI has been largely proven to affect the seismic response, especially in the case of short piers and soft soils [2-7]. Concerning OWTs, the main effects of SSI is the change of the fundamental frequency and damping of the foundation-structure system with respect to the fixed-base condition, which may lead to resonance problems with the rotor and the blade-passing frequencies. The former corresponds to rotor or aerodynamic unbalance loads, while the latter is produced by the shadowing effect from the wind of the blades passing the tower. Usually, codes recommend keeping the tower frequency outside the ±10% range of these frequencies and suggest different design approaches depending on the ratio between the tower fundamental frequency and the aforementioned frequencies [8-10]. Thus, SSI effects should be carefully considered in the design, especially in the case of monopile foundations. In addition, recent studies demonstrated that SSI may also play an important role on the seismic response of OWTs, leading to beneficial or detrimental effects depending on the size of the rated power [11-16].

In the framework of the substructure approach [17], SSI effects on the seismic and non-seismic response of bridges and OWTs can be evaluated by modelling superstructures on compliant bases. For seismic actions, superstructures are subjected to the Foundation Input Motion (FIM), i.e. the motion experienced by the foundation due to the propagation of the seismic waves into the soil (kinematic interaction). The soil-foundation impedances, namely the frequency-dependent force-displacement relationships that govern the behaviour of the compliant restraints, as well as the FIM are determined through the analysis of the soil-foundation subdomain. The same analysis also provides kinematic stress resultants in the foundation elements.

With both references to floating and end-bearing piles, the problem of the dynamic soil-foundation interaction analysis has been widely addressed in the literature with the aim of providing analytical or numerical solutions for impedances and FIM. On the contrary, caisson foundations have been primarily investigated for what concern their load vertical and lateral capacity, while the dynamic response has received less attention. One of the first works dealing with the vibration problem of embedded foundations is the one by Beredugo and Novak [18], in which an approximate analytical solution was developed to predict the coupled horizontal and rocking vibration by assuming the foundation to be rigid. Later, Veletsos et al. [19] analysed the dynamic modelling and response of rigid cylinders supported by a non-deformable rigid base and embedded in a uniform viscoelastic stratum of constant thickness and infinite extent in the horizontal direction. Under the same assumptions, Saitoh and Watanabe [20] presented a detailed investigation of the influence on the rocking impedance of flexible sidewalls in embedded foundations. Gerolymos and Gazetas contributed to the problem in 2005, developing a Winkler model for the analysis of the static and dynamic response of rigid caisson foundations, also addressing the problem of nonlinearities at the soil-caisson interface [21, 22]. In the same year, Beltrami et al. [23] studied the kinematic interaction problem of rigid large-diameter shaft foundations developing an analytical model using solutions of rigid walls and fixed base cylinders subjected to a dynamic excitation. The above studies investigated the response of embedded cylindrical foundations mainly through an analytical approach, by making suitable simplifying assumptions such as the ones relevant to the soil stratigraphy, the caisson base restraints, or the analysis of some specific components of the soil-foundation impedance matrix. The impedances of flexible caissons were studied in 2007 by Liingaard et al. [24] through a three-dimensional coupled boundary element/finite element model of the soil-foundation system, assuming the soil as a linear homogeneous viscoelastic material. The authors also compared their results with those obtained from known analytical and numerical solutions and carried out a parametric investigation by varying the main geometric and mechanical parameters affecting the system response. Following the approach by Liingaard et al. [24], more recently, a significant number of papers were published investigating the kinematic interaction of caissons foundations exploiting a finite element modelling approach, taking advantage of the continuous IT advances leading to ever more performing computers [25-29]. However, despite high performant computers are nowadays available, finite element or boundary element modelling strategies still remain computationally demanding procedures for the analysis of SSI problems because a significant portion of soil (usually not only the near-field portion) must be included in the models due to the non-perfect radiation condition at the model boundaries, which is usually simulated numerically through infinite elements or Lysmer-Kuhlemeyer dashpots [30]. Consequently, the above methods are not suitable for phenomenological or probabilistic investigations of the dynamic response of caisson foundations on a large scale, since they imply a parametric scheme to study the effects on impedances and on the FIM due to the variability of the geometric and mechanical parameters of the problem, which may be very high, especially if stratified soil conditions are taken into account. For the same reasons they are not feasible for applications in frameworks for the seismic risk assessment of structures and infrastructures on regional scale, where fragility curves derived from the probabilistic analysis of the vulnerability of archetype structural systems are needed. In this case, the absence of data deriving from soil in-situ and laboratory tests of a specific case study, as well as the need to perform thousands of applications to derive fragility curves according to a probabilistic scheme, make it impossible to perform comprehensive nonlinear soil-foundation-structure interaction analyses, and simplified linear or linear equivalent models must be suitably adopted to include SSI effects in the fragility analyses, risk evaluation and loss assessments. In addition, nonlinear sophisticated models are redundant for seismic verifications of structures at damageability limit states and results of linear models are fundamental to validate those achieved from nonlinear ones. Above considerations suggest that, despite the current computing power allow performing complex nonlinear analyses, linear applications retain their usefulness in both research and practical applications.

In this work, a Winkler-based analytical model for the analysis of the dynamic response of caissons foundations is developed. The model is conceived to be used in the framework of the sub-structuring method for the seismic analysis of SSI problems, providing both impedances and the kinematic response of soil-caisson systems embedded in layered soil deposits. Thus, the model permits exploiting the well-known advantages of the sub-structuring method, including the possibility of using different dedicated software for the analysis of the soil-foundation and the superstructure systems, and the possibility to include the superstructure nonlinearities in the inertial interaction analysis.

The caisson is modelled as a Timoshenko beam and the soil-caisson interactions are introduced through functions expressing the soil reactions as a function of the relative displacement between the caisson and the soil. The latter are obtained from the solution of a rigid annular cross-section vibrating in an infinite homogeneous soil layer. The steady or transient dynamic excitation is represented by the soil free-field displacements, which may be computed considering a linear equivalent approach to account for the soil nonlinearities by defining secant soil shear moduli and damping rations, consistent with strains attained during the motion, that can be also used to express the soil-caisson interaction forces. The problem solution is obtained numerically through a finite element approach. The model is characterised by few degrees of freedom since the soil is not physically included in the formulation and the solution is characterised by a very low computational demand, which makes it consistent with the need of iterative analyses if the soil nonlinearities need to be considered through a linear-equivalent approach. The model efficiency in capturing impedances and the kinematic response of caisson foundations is tested through comparisons of results with those provided by a rigorous model based on coupling the Boundary Element Method (BEM) and the Finite Element Method (FEM) [31,37], and some limits of the developed tool are addressed and discussed. The model revealed suitable for a large-scale phenomenological investigation of the kinematic response of caisson foundations in homogeneous or stratified media, by varying the soil-foundation parameters (e.g. soil stratigraphy, soil mechanical properties, caisson length, skirt thickness). Also, the reliability of the proposed model in predicting the seismic response of these foundations is tested through some applications involving realistic caisson foundations and real earthquakes.

2 PROPOSED WINKLER MODEL

A single cylindrical caisson foundation embedded in a horizontally layered soil deposit and subjected to the free-field seismic soil displacements is considered. The foundation has a diameter D and a thickness of the skirt s. The problem is formulated in the frequency domain by assuming a linear viscoelastic behaviour for the caisson and the soil (Figure 1a). Perfectly bonded contact conditions between soil and skirt are assumed while the soil-lid contact is neglected.

2.1 Kinematics

A global orthonormal reference system frame $\{0, x_1, x_2, z\}$, with the origin at the centroid of the top plane of the stratum and the z axis directed downward, is defined as in Figure 1a.

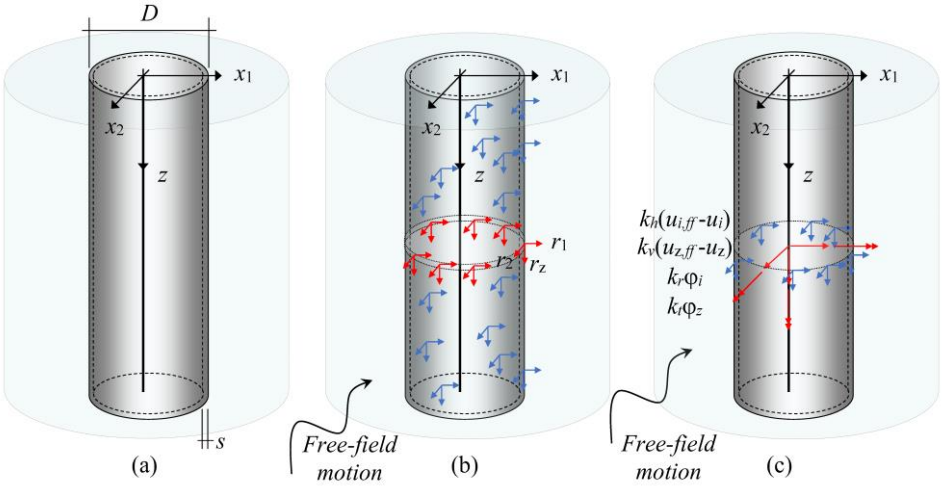

Figure 1. (a): Caisson foundation embedded in the horizontally layered soil profile; (b) foundation subjected to interaction forces and (c) resultants of interactions forces (red forces) at a certain depth due to the Winkler's assumption.

According to the Timoshenko beam theory, the displacements of a generic point p of coordinates x_1, x_2 and z can be expressed by the following complex valued functions, starting from the displacements of the cross-section centroids:

$$u_{z,p}(\omega; x_1, x_2, z) = u_z(\omega; z) + \varphi_1(\omega; z)x_2 - \varphi_2(\omega; z)x_1 \quad (1a)$$

$$u_{1,p}(\omega; x_1, x_2, z) = u_1(\omega; z) - \varphi_z(\omega; z)x_2 \quad (1b)$$

$$u_{2,p}(\omega; x_1, x_2, z) = u_2(\omega; z) + \varphi_z(\omega; z)x_1 \quad (1c)$$

in which $u_{z,p}$, $u_{1,p}$ and $u_{2,p}$ are the displacements along the vertical and horizontal directions x_1 and x_2, respectively. In Equation (1), displacements of the cross-section centroids are expressed by u_1 and u_2 (horizontal displacements in x_1 and x_2 directions, respectively), φ_1 and φ_2 (rotations about x_1 and x_2 axes, respectively), and u_z and φ_z (displacement and rotation along and around the vertical z axis, respectively). The pile non-null strains are obtained from displacements (1) and are expressed by

$$\varepsilon_z(\omega; x_1, x_2, z) = u_z' + \varphi_1' x_2 - \varphi_2' x_1 \tag{2a}$$
$$\gamma_{1z}(\omega; x_1, x_2, z) = u_1' - \varphi_z' x_2 - \varphi_2 \tag{2b}$$
$$\gamma_{2z}(\omega; x_1, x_2, z) = u_2' + \varphi_z' x_1 + \varphi_1 \tag{2c}$$

in which prime denotes derivatives with respect to z.

2.2 The linear dynamic problem

By assuming a linear behaviour for the foundation, the dynamic problem can be expressed through the Lagrange D'Alembert principle, assuming that the work resulting from external and inertia forces acting through every virtual consistent displacement field is equal to that resulting from stresses acting through every virtual strain field. External forces develop during the motion along the cross-section boundaries due to soil-pile interactions. Unknown interaction forces $r_1(\omega; x_1, x_2, z)$, $r_2(\omega; x_1, x_2, z)$ and $r_z(\omega; x_1, x_2, z)$ along x_1, x_2 and z directions, respectively (red forces in Figure 2b), are herein defined; assuming that no gaps arise during the motion, forces at a generic depth z result from the non-local soil-pile interaction, depending on displacements occurring over the whole caisson lateral surface (blue forces in Figure 2b). In addition, inertia forces develop during the motion, depending on the caisson density ρ. The Lagrange d'Alembert principle provides the following balance condition:

$$\begin{aligned}&\int_0^L (EAu_z'\delta u_z' + EI\varphi_1'\delta\varphi_1' + EI\varphi_2'\delta\varphi_2' + \\ &+\frac{GA}{\chi}[(u_1' - \varphi_2)(\delta u_1' - \delta\varphi_2) + (u_2' + \varphi_1)(\delta u_2' + \delta\varphi_1)] + GI_p\varphi_z'\delta\varphi_z'\Big)dz = \omega^2 \int_0^L \big(\rho A u_1\delta u_1 + \\ &\rho A u_2\delta u_2 + \rho A u_z\delta u_z + \rho I\varphi_1\delta\varphi_1 + \rho I\varphi_2\delta\varphi_2 + \rho I_p\varphi_z\delta\varphi_z\big)dz + \int_0^L\int_{\partial A}\big(r_1\delta(u_1 - x_2\varphi_z) + \\ &r_2\delta(u_2 + x_1\varphi_z) + r_z\delta(u_z + x_2\varphi_1 - x_1\varphi_2)\big)ds\,dz \\ &\forall\delta\bullet(z) \neq 0\end{aligned} \tag{3}$$

In Equation (3), E and G are the Young's and shear modulus of the material of the cross-section of the caisson foundation while A and I are the area and the moment of the inertia of the circular annular cross-section around a principal axis. In addition, $I_p = 2I$ is the polar moment of inertia and χ is the shear corrector factor. Equation (3) cannot be solved since the soil-caisson interaction forces depends on the unknown displacement field on the overall lateral surface of the caisson. The problem can be simplified by introducing the Winkler's assumption, namely by assuming that the interactions forces at depth z depends only on displacements at the same depth (Figure 2c); by considering a linear viscoelastic behaviour for the soil, the resultants of the interaction forces at depth z are derived in the following section considering the harmonic vibration of an embedded rigid body with annular cross-section.
By defining with $u_{1,ff}(z;\omega)$, $u_{2,ff}(z;\omega)$ and $u_{3,ff}(z;\omega)$ the translational components of the free-field motion along the x_1, x_2 and z directions, respectively, the soil-pile interaction forces can be expressed exploiting impedances obtained from the solution of the vibration problem of the rigid annular cross-section, which allows obtaining the following form for the balance condition:

$$\begin{aligned}&\int_0^L (EAu_z'\delta u_z' + EI\varphi_1'\delta\varphi_1' + EI\varphi_2'\delta\varphi_2' \\ &+\frac{GA}{\chi}[(u_1' - \varphi_2)(\delta u_1' - \delta\varphi_2) + (u_2' + \varphi_1)(\delta u_2' + \delta\varphi_1)] + GI_p\varphi_z'\delta\varphi_z'\Big)dz - \omega^2 \int_0^L \big(\rho A u_1\delta u_1 + \rho A u_2\delta u_2 + \\ &\rho A u_z\delta u_z + \rho I\varphi_1\delta\varphi_1 + \rho I\varphi_2\delta\varphi_2 + \rho I_p\varphi_z\delta\varphi_z\big)dz + \int_0^L (k_h u_1\delta u_1 + k_h u_2\delta u_2 + k_v u_z\delta u_z + k_r\varphi_1\delta\varphi_1 + \\ &k_r\varphi_2\delta\varphi_2 + k_t\varphi_z\delta\varphi_z)dz = \int_0^L \big(k_h u_{1,ff}\delta u_1 + k_h u_{2,ff}\delta u_2 + k_v u_{z,ff}\delta u_z\big)dz \quad \forall\delta\bullet(z) \neq 0\end{aligned} \tag{4}$$

It is worth observing that the soil-pile interaction forces depend on the difference between displacements of the caissons foundations and those experienced by the soil without the caisson (i.e. the free-field motion). The balance condition can be written in the following compact form

$$\begin{aligned}&\int_0^L \mathbf{K}\boldsymbol{\mathcal{D}}\mathbf{u}(\omega; z)\cdot\delta\boldsymbol{\mathcal{D}}\mathbf{u}(z)dz - \omega^2\int_0^L \mathbf{M}\mathbf{u}(\omega; z)\cdot\delta\mathbf{u}(z)dz + \int_0^L \mathbf{K}_s(\omega; z)\mathbf{u}(\omega; z)\cdot\delta\mathbf{u}(z)dz = \\ &\int_0^L \mathbf{K}_s(\omega; z)\mathbf{u}_{ff}(\omega; z)\cdot\delta\mathbf{u}(z)dz \qquad \forall\delta\mathbf{u}(z) \neq \mathbf{0}\end{aligned} \tag{5}$$

where

$$\mathbf{u}(\omega; z) = [u_1 \quad u_2 \quad u_3 \quad \varphi_1 \quad \varphi_2 \quad \varphi_z]^T \tag{6a}$$

$$\mathbf{u}_{ff}(\omega; z) = [u_{1,ff} \quad u_{2,ff} \quad u_{3,ff} \quad 0 \quad 0 \quad 0]^T \tag{6a}$$

are the vectors collecting displacements of the caisson axis at depth z, and the vector of the free-field motion, respectively, and

$$\boldsymbol{K} = \begin{bmatrix} GA\chi^{-1} & 0 & 0 & 0 & 0 & 0 \\ 0 & GA\chi^{-1} & 0 & 0 & 0 & 0 \\ 0 & 0 & EA & 0 & 0 & 0 \\ 0 & 0 & 0 & EI & 0 & 0 \\ 0 & 0 & 0 & 0 & EI & 0 \\ 0 & 0 & 0 & 0 & 0 & GI_p \end{bmatrix} \tag{7a}$$

$$\boldsymbol{M} = \rho \begin{bmatrix} A & 0 & 0 & 0 & 0 & 0 \\ 0 & A & 0 & 0 & 0 & 0 \\ 0 & 0 & A & 0 & 0 & 0 \\ 0 & 0 & 0 & I & 0 & 0 \\ 0 & 0 & 0 & 0 & I & 0 \\ 0 & 0 & 0 & 0 & 0 & I_p \end{bmatrix} \tag{7b}$$

are the stiffness and mass matrices of the caisson cross-section. In addition,

$$\mathbf{K}_s = \begin{bmatrix} k_h & 0 & 0 & 0 & 0 & 0 \\ 0 & k_h & 0 & 0 & 0 & 0 \\ 0 & 0 & k_v & 0 & 0 & 0 \\ 0 & 0 & 0 & k_r & 0 & 0 \\ 0 & 0 & 0 & 0 & k_r & 0 \\ 0 & 0 & 0 & 0 & 0 & k_t \end{bmatrix} \tag{8}$$

$$\boldsymbol{\mathcal{D}} = \begin{bmatrix} \frac{d}{dz} & 0 & 0 & 0 & -1 & 0 \\ 0 & \frac{d}{dz} & 0 & 1 & 0 & 0 \\ 0 & 0 & \frac{d}{dz} & 0 & 0 & 0 \\ 0 & 0 & 0 & \frac{d}{dz} & 0 & 0 \\ 0 & 0 & 0 & 0 & \frac{d}{dz} & 0 \\ 0 & 0 & 0 & 0 & 0 & \frac{d}{dz} \end{bmatrix} \tag{9}$$

are the soil impedance matrix and a differential operator, respectively.

2.3 Soil reactions for the rigid annular cross-section

The key ingredient of a Winkler-based model is the use of appropriate and physically relevant soil reactions due to the foundation movement, i.e., the correct selection of types and values of distributed springs and dashpots for the problem at hand. In this regard, there is a vast literature where these are obtained analytically or via curve fitting of numerical results for many different foundation configurations, see e.g. the literature review in [42]. In the context of the dynamic analysis of pile foundations, one of the most widely known expressions is the plane strain solution of Novak et al. [43], where vertical, torsional, horizontal, and rotational soil reactions of an infinitely long cylinder are obtained in closed-form formulas. Despite neglecting three-dimensional phenomena, these plane strain soil reactions work reasonably well for floating slender solid piles even for stratified soils [44], although, for some of them, the stiffness approaches zero when $\omega \to 0$. A straightforward workaround of this drawback is the use a constant stiffness for frequencies below some threshold as proposed by Novak and Sheta [45] ($k(a_0) = k(0.3)$ when dimensionless frequency $a_0 < 0.3$ for the problematic components).

In the case of caissons and short piles, it is quite reasonable to argue that the physics of the soil inside the foundation may play a relevant role in the foundation response due to the relevant mass and stiffness of the inner soil column restricted by the skirt of the caisson foundation. This inner soil column will be characterized by its own dynamic properties, and will interact with the rest of the system, Thus, the effects of the inner soil on the system dynamics should be somehow included in a Winkler model. With this idea in mind, in this work Novak's soil reactions are complemented with a new set of soil reactions related to the internal soil. This means that a foundation with rigid annular cross-section containing external and internal soil is considered, see Figure 2. Plane strain conditions allow obtaining up to four modes of soil reactions: vertical, torsional, horizontal, and rotational; see Figure 3. The solution to each soil reaction mode can be obtained by conveniently solving time harmonic Navier equation. Due to the geometrical nature of the problem, the

equations are decoupled by using a method of potentials and cylindrical coordinates as proposed by Pak [39]. The resulting three uncoupled wave equations, together with the appropriate boundary conditions, are used to solve tractions along the soil-foundation interface. Soil reaction for each mode is obtained by integration of the relevant tractions along the soil-foundation interface. The resulting closed-form formulas are presented in Table 1, where it should be noticed that the expressions are similar to those of Novak, except for some factors and the presence of the modified Bessel function $I_m(z)$ instead of $K_m(z)$.

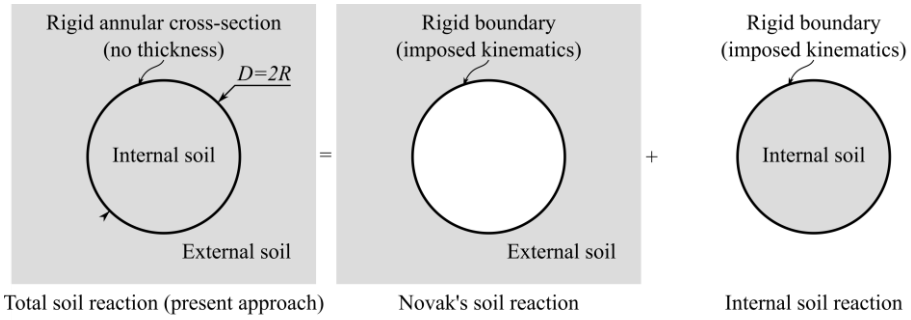

Figure 2. Soil reactions considered in the proposed model

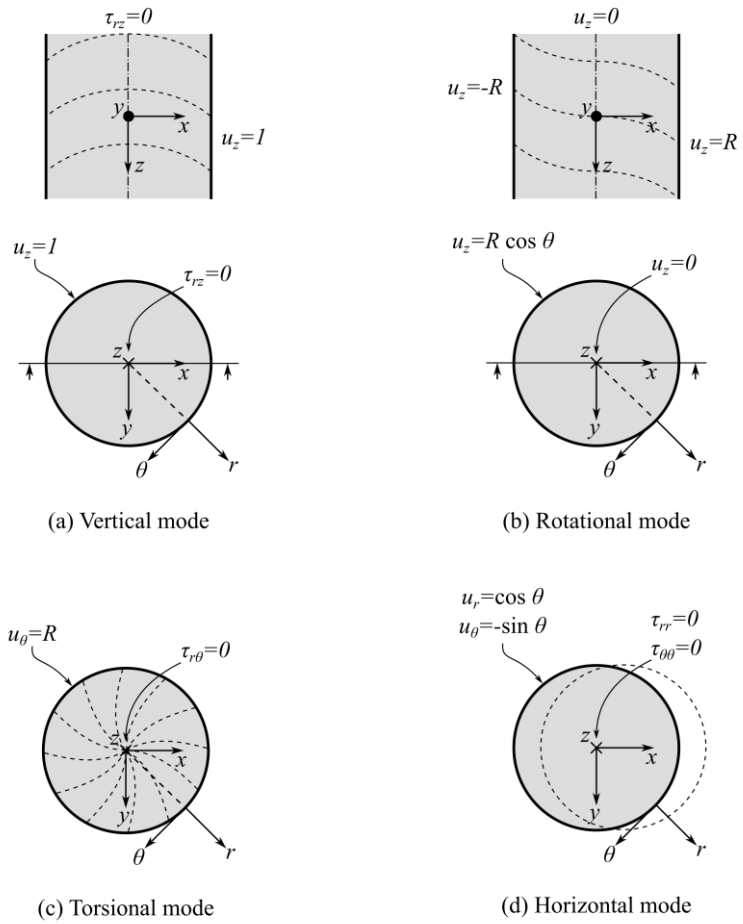

Figure 3. Internal soil reaction modes and their corresponding boundary conditions.

Table 1. Closed-form formulas of soil reaction modes. λ, G and ρ are the Lamé's first parameter, shear modulus and density of the soil, respectively. $R = D/2$ is the radius of the foundation. S-wave dimensionless frequency is $a_s = i\omega R/V_s$, where $V_s = \sqrt{G/\rho}$. P-wave dimensionless frequency is $a_p = i\omega R/V_p$, where $V_p = \sqrt{(\lambda + 2\mu)/\rho}$. Hysteretic damping is introduced via the usual complex λ and G in the previous equations. Modified Bessel functions of m-th order are denoted as $I_m^s = I_m(a_s)$, s $I_m^p = I_m(a_p)$, $K_m^s = K_m(a_s)$ and $K_m^p = K_m(a_p)$.

Mode	**Internal soil**	**External soil [43]**
Vertical (k_v)	$2\pi G a_s \frac{I_1^s}{I_0^s}$	$2\pi G a_s \frac{K_1^s}{K_0^s}$
Torsional (k_t)	$2\pi G R^2 \left(a_s \frac{I_0^s}{I_1^s} - 2\right)$	$2\pi G R^2 \left(a_s \frac{K_0^s}{K_1^s} + 2\right)$
Horizontal (k_h)	$-\pi G a_s^2 \frac{a_s I_0^s I_1^p + a_p I_0^p I_1^s - 4 I_1^s I_1^p}{a_s I_0^s I_1^p + a_p I_0^p I_1^s - a_s a_p I_0^s I_0^p}$	$\pi G a_s^2 \frac{a_s K_0^s K_1^p + a_p K_0^p K_1^s + 4 K_1^s K_1^p}{a_s K_0^s K_1^p + a_p K_0^p K_1^s + a_s a_p K_0^s K_0^p}$
Rotational (k_r)	$\pi G R^2 \left(a_s \frac{I_0^s}{I_1^s} - 1\right)$	$\pi G R^2 \left(a_s \frac{K_0^s}{K_1^s} + 1\right)$

2.4 Finite element solution

The solution of the problem may be achieved numerically by the finite element method in the displacement-based approach, by dividing the caisson axis into *e* elements and approximating the displacements within the elements by interpolating those of the end nodes. An interdependent interpolation element is considered for the Timoshenko beam model while linear interpolating functions are adopted for axial and torsional displacements. According to the finite element method, the pile displacements may be approximated as

$$\mathbf{u}(\omega; z) \cong \mathbf{N}(z)\mathbf{d}^{\boldsymbol{e}}(\omega) \tag{10}$$

where

$$\mathbf{d}^e(\omega) = [u_{1h} \quad u_{2h} \quad u_{zh} \quad \varphi_{1h} \quad \varphi_{2h} \quad \varphi_{zh} \quad u_{1k} \quad u_{2k} \quad u_{zk} \quad \varphi_{1k} \quad \varphi_{2k} \quad \varphi_{zk}]^T \tag{11}$$

is the nodal displacement vector of the generic element having end nodes *h* and *k* and

$$\mathbf{N}(z) = \begin{bmatrix} n_1 & 0 & 0 & 0 & -n_2 & 0 & n_3 & 0 & 0 & 0 & -n_4 & 0 \\ 0 & n_1 & 0 & n_2 & 0 & 0 & 0 & n_3 & 0 & n_4 & 0 & 0 \\ 0 & 0 & n_8 & 0 & 0 & 0 & 0 & 0 & n_9 & 0 & 0 & 0 \\ 0 & n_5 & 0 & n_6 & 0 & 0 & 0 & -n_5 & 0 & n_7 & 0 & 0 \\ -n_5 & 0 & 0 & 0 & n_6 & 0 & n_5 & 0 & 0 & 0 & n_7 & 0 \\ 0 & 0 & 0 & 0 & 0 & n_8 & 0 & n_5 & 0 & 0 & 0 & n_9 \end{bmatrix} \tag{12}$$

is the matrix of the interpolating polynomials. In Equation (12)

$$n_1(z, \Omega) = \frac{1}{1+12\Omega}\left[2\left(\frac{z}{L_e}\right)^3 - 3\left(\frac{z}{L_e}\right)^2 - 12\Omega\left(\frac{z}{L_e} - 1\right) + 1\right] \tag{13a}$$

$$n_2(z, \Omega) = -\frac{L_e}{1+12\Omega}\left(\frac{z}{L_e}\right)\left[\left(1 - \frac{z}{L_e}\right)^2 + 6\Omega\left(1 - \frac{z}{L_e}\right)\right] \tag{13b}$$

$$n_3(z, \Omega) = \frac{1}{1+12\Omega}\left[3\left(\frac{z}{L_e}\right)^2 - 2\left(\frac{z}{L_e}\right)^3 + 12\Omega\frac{z}{L_e}\right] \tag{13c}$$

$$n_4(z, \Omega) = \frac{L_e}{1+12\Omega}\left(\frac{z}{L_e}\right)\left[\left(\frac{z}{L_e}\right) - \left(\frac{z}{L_e}\right)^2 + 6\Omega\left(1 - \frac{z}{L_e}\right)\right] \tag{13d}$$

$$n_5(z, \Omega) = \frac{6}{L_e(1+12\Omega)}\left(\frac{z}{L_e}\right)\left(1 - \frac{z}{L_e}\right) \tag{13e}$$

$$n_6(z, \Omega) = \frac{1}{1+12\Omega}\left[1 + 3\left(\frac{z}{L_e}\right)^2 - 4\left(\frac{z}{L_e}\right) + 12\Omega\left(1 - \frac{z}{L_e}\right)\right] \tag{13f}$$

$$n_7(z, \Omega) = \frac{1}{1+12\Omega}\left[3\left(\frac{z}{L_e}\right)^2 - 2\left(\frac{z}{L_e}\right) + 12\Omega\left(\frac{z}{L_e}\right)\right] \tag{13g}$$

$$n_8(z) = \left(1 - \frac{z}{L_e}\right) \tag{13h}$$

$$n_9(z) = \frac{z}{L_e} \tag{13i}$$

where L_e is the length of the finite element, and

$$\Omega = \frac{EJ\chi}{GAL_e^2} \tag{14}$$

By considering the approximation (10) and the contribution of all the elements, the global balance condition (5) becomes

$$\sum_{e=1}^{E}\int_0^{L_e}(\mathcal{D}\mathbf{N})^T\mathbf{K}\mathcal{D}\mathbf{N}\mathbf{d}^e\cdot\delta\mathbf{d}^e dz\ -\omega^2\sum_{e=1}^{E}\int_0^{L_e}(\mathbf{N})^T\mathbf{M}\mathbf{N}\mathbf{d}^e\cdot\delta\mathbf{d}^e dz+\sum_{e=1}^{E}\int_0^{L_e}(\mathbf{N})^T\mathbf{K}_s\mathbf{N}\mathbf{d}^e\cdot\delta\mathbf{d}^e dz = \sum_{e=1}^{E}\int_0^{L_e}(\mathbf{N})^T\mathbf{K}_s\mathbf{u}_{ff}\cdot\delta\mathbf{d}^e dz \qquad \forall\delta\mathbf{d}^e\neq\mathbf{0} \tag{15}$$

By suitably assembling the node displacements in a unique displacement vector **d**(ω), standard considerations make it possible to obtain the complex linear equation system

$$\left(\mathbf{K}_p-\omega^2\mathbf{M}_p+\mathbf{K}_f\right)\mathbf{d}=\mathbf{f} \tag{16}$$

where

$$\mathbf{K}_p=\sum_{e=1}^{E}\int_0^{L_e}(\mathcal{D}\mathbf{N})^T\mathbf{K}\mathcal{D}\mathbf{N}dz \tag{17}$$

$$\mathbf{M}_p=\sum_{e=1}^{E}\int_0^{L_e}(\mathbf{N})^T\mathbf{M}\mathbf{N}dz \tag{18}$$

$$\mathbf{K}_f=\sum_{e=1}^{E}\int_0^{L_e}(\mathbf{N})^T\mathbf{K}_s\mathbf{N}dz \tag{19}$$

are the global stiffness matrix and the global mass matrix of the foundation, and the global impedance matrix of the soil, obtained by assembling the relevant contributions of all the elements, and

$$\mathbf{f}=\sum_{e=1}^{E}\int_0^{L_e}(\mathbf{N})^T\mathbf{K}_s\mathbf{u}_{ff}dz \tag{20}$$

is the vector of the external loads due to the free-field motion.

2.5 Impedances and kinematic response functions

System (16) can be partitioned as follows to highlight displacements of the head node of the caisson, collected in the vector $\mathbf{d}_h$, from those of the remaining embedded nodes $\mathbf{d}_e$:

$$\begin{bmatrix}\mathbf{K}_{hh} & \mathbf{K}_{he}\\ \mathbf{K}_{eh} & \mathbf{K}_{ee}\end{bmatrix}\begin{bmatrix}\mathbf{d}_h\\ \mathbf{d}_e\end{bmatrix}=\begin{bmatrix}\mathbf{f}_h\\ \mathbf{f}_e\end{bmatrix} \tag{21}$$

In Equation (21), $\mathbf{f}_h$ and $\mathbf{f}_e$ collects soil-caisson interaction forces acting at the head, and at the embedded nodes, respectively, and

$$\begin{bmatrix}\mathbf{K}_{hh} & \mathbf{K}_{he}\\ \mathbf{K}_{eh} & \mathbf{K}_{ee}\end{bmatrix}=\left(\mathbf{K}_p-\omega^2\mathbf{M}_p+\mathbf{K}_f\right) \tag{22}$$

After simple manipulations, the following equation is obtained

$$(\mathbf{K}_{hh}-\mathbf{K}_{he}\mathbf{K}_{ee}^{-1}\mathbf{K}_{eh})\mathbf{d}_h=\mathbf{f}_h-\mathbf{K}_{he}\mathbf{K}_{ee}^{-1}\mathbf{f}_e \tag{23}$$

from which

$$\mathfrak{J}(\omega)=\mathbf{K}_{hh}-\mathbf{K}_{he}\mathbf{K}_{ee}^{-1}\mathbf{K}_{eh} \tag{24}$$

is the complex valued foundation impedance matrix. Finally, the motion of the head node (FIM) may be expressed as

$$\mathbf{d}_h(\omega) = \mathfrak{F}^{-1}(\mathbf{f}_h - \mathbf{K}_{he}\mathbf{K}_{ee}^{-1}\mathbf{f}_e) \tag{25}$$

3 MODEL VALIDATION

This section provides a validation of the proposed model through an extensive comparison of the model results with those resulting from a rigorous BEM-FEM modelling of the soil-caisson interaction problem. Comparisons are aimed to provide an overview of the model ability in capturing both the impedances and the kinematic response of caisson foundations, discussing its applicability as a function of the system parameters and the relevant degree of accuracy.

3.1 Reference BEM-FEM model

For the sake of validation, the proposed model is compared against a previously developed model based on coupling the BEM and the FEM [31,37]. Within the context of linear dynamic analyses, this numerical model is a rigorous physical representation of the problem. On one hand, the foundation skirt and lid are modeled through well-established shell finite elements [38]. On the other hand, the soil is modeled using the BEM, where boundary elements and body load elements are coupled with shell finite elements under perfectly welded conditions. As it is well known, the main ingredient of the BEM is Green's functions, and, in this case, the Green's function of Pak and Guzina [39] for a stratified viscoelastic half-space is used. In the following, a summary of the formulation is given.

Shell FEM modeling of the foundation is based on the usual element equilibrium equation [40], which for an element *e* can be written as:

$$\left(\mathbf{K}^{(e)} - \omega^2\mathbf{M}^{(e)}\right) \cdot \mathbf{a}^{(e)} - \mathbf{Q}^{(e)} \cdot \mathbf{p}^{(e)} = \mathbf{q}^{(e)} \tag{26}$$

where $\mathbf{K}^{(e)}$ and $\mathbf{M}^{(e)}$ are the stiffness and mass matrices, $\mathbf{a}^{(e)}$ gathers the element degrees of freedom (displacements and rotations for each element node), $\mathbf{Q}^{(e)}$is the matrix that transforms mid-surface distributed loads $\mathbf{p}^{(e)}$ into equivalent nodal loads, and $\mathbf{q}^{(e)}$is the element equilibrating load vector. Element stiffness matrix is obtained from the locking-free MITC methodology [38], while the rest of the matrices result from the standard shell, obtained from the degeneration of the solid approach. Global FEM equations are obtained from the usual assemblage procedure.

Soil is modeled by using the BEM. BEM equations are built by appropriate collocation of boundary integral equations [41]:

$$c_{lk}^i u_k^i + \int_{\Gamma_{\text{lid}}} t_{lk}^* u_k d\Gamma = \int_{\Gamma_{\text{lid}}} u_{lk}^* t_k d\Gamma + \int_{\Gamma_{\text{skirt}}} u_{lk}^* b_k d\Gamma \tag{27}$$

where indicial notation $l, k = 1,2,3$ and Einstein summation is implied. The free-term c_{lk}^i is related to the local geometry around the collocation point, while u_k^i is the displacement at the collocation point. Green's function in terms of displacements and tractions are u_{lk}^* and t_{lk}^*, respectively. Displacements and tractions along the domain boundaries are u_k and t_k, which, due to the use of the stratified half-space Green's function, is reduced only to the foundation lid Γ_{lid} (if present). Likewise, the discretization of the free-surface and the interfaces between soil layers are no longer required. Foundation skirt can be represented through displacements u_k and surface body loads b_k along its mid-surface Γ_{skirt}. Finally, perfectly welded contact conditions between soil and foundation are established by imposing compatibility and equilibrium at each node n:

$$[u_k^{(n)}]_{\text{foundation}} = [u_k^{(n)}]_{\text{soil}} \tag{28}$$

$$[p_k^{(n)}]_{\text{foundation-lid}} + [t_k^{(n)}]_{\text{soil-lid}} = 0 \tag{29}$$

$$[p_k^{(n)}]_{\text{foundation-skirt}} + [b_k^{(n)}]_{\text{soil-skirt}} = 0 \tag{30}$$

This model is built in two flavors: foundation with lid (typical of suction caissons, where lid interaction may occur), and foundation without lid (typical of short monopiles, where lid interaction is not present). Figure 4 shows a graphical summary of the resulting BEM-FEM coupled model, where the geometrically coincident elements are exploded for the sake of clarity. As shown in the figure, due to the symmetry of the problem only one quarter of the domain needs to be discretized.

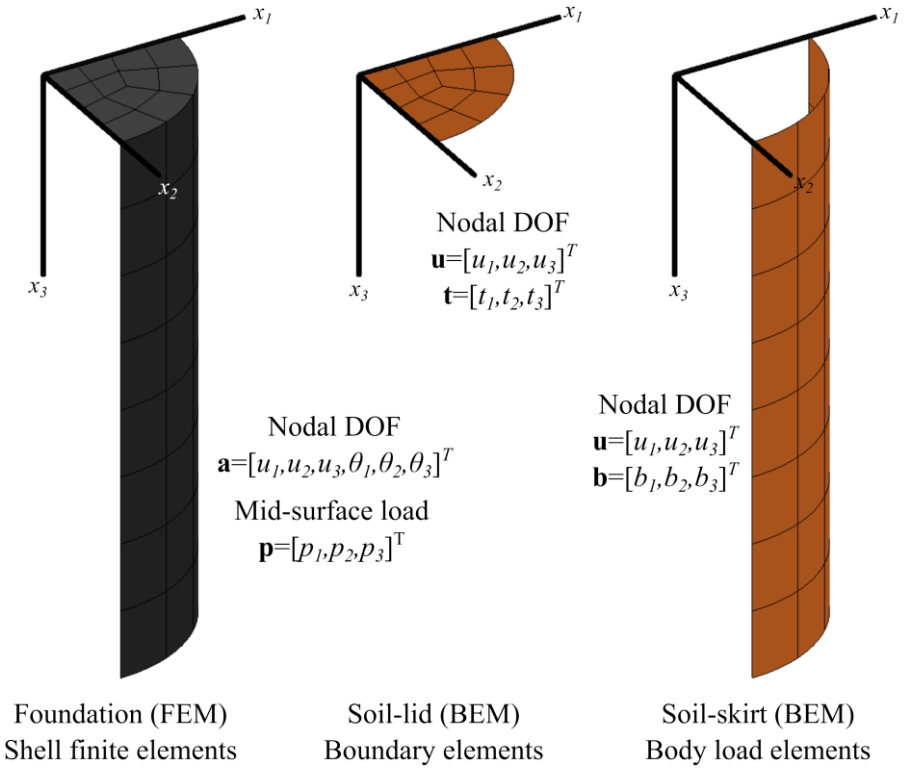

Figure 4. Graphical summary of the BEM-FEM model

3.2 Definition of the parametric investigation

The model validation is achieved through a parametric analysis performed by varying the material of the caisson, which is assumed to be made of reinforced Concrete (C) or Steel (S), the length/diameter ratio (L/D), the skirt thickness/diameter ratio (s/D), and the shear wave velocity ($V_s(z)$) profile of the soil deposit. Two models are considered for the latter: a constant shear wave velocity profile to represent a Homogeneous (H) deposit, or a model characterized by an Exponential trend (E) of the shear wave velocity profile, to simulate the progressive increase of the soil dynamic properties with depth (Figure 5). The soil stiffness is expressed in terms of the shear wave velocity $V_{s,D}$, which is assumed to be 100, 175 and 250 m/s. In detail, the following formulation is defined for the shear wave velocity profile:

$$V_s(z) = V_{s,D}\left(\frac{z+0.2}{D+0.2}\right)^{\alpha} \tag{31}$$

where $V_s(z)$ is the depth-dependent shear wave velocity, z is the vertical abscissa of the soil measured from the surface, and $V_{s,D}$ is the reference shear wave velocity at a depth $z = D$. α is a parameter governing the shape of the velocity profile: for $\alpha = 0$ a homogeneous soil with constant shear wave velocity $V_{s,D}$ is obtained while $\alpha = 0.25$ provides an exponential trend characterised by a shear wave velocity $V_{s,D}$ at depth of one diameter. It is worth noting that the exponential trend is characterised by a non-null value of the shear wave velocity at $z = 0$, to simulate a realistic soil condition (Figure 5).

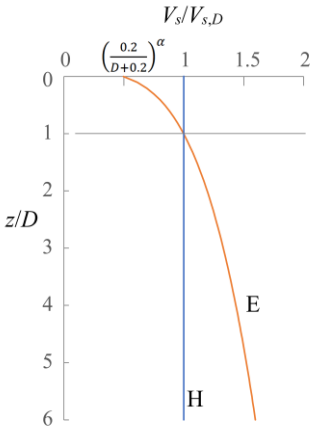

Figure 5. Scheme of the soil deposits.

The skirt thickness/diameter ratio (s/*D*) is fixed to 0.01 for steel caissons (S) and to 0.1 for concrete caissons (C), while the length/diameter ratio (*L*/*D*) is varied between 2, 4 and 6. All the parameters of the parametric investigation are summarized in Table 2.

Table 1: Parameters adopted for the investigation

Caisson material	***s/D***	***L/D***	**Soil profile**	$V_{s,D}$
Steel (S)	0.01	2, 4, 6	H, E	100, 175, 250
Reinforced Concrete (C)	0.1	2, 4, 6	H, E	100, 175, 250

The parameter combination generates a total number of 36 case studies that cover a wide range of possible situations (short to medium steel or reinforced concrete caissons in very soft or medium-stiff soils). In the sequel, each case study is labelled according to the following rule: Material_*L/D*&soil profile_ V_s so that, for example, the case S_2H_100 identifies a steel caisson of length equal to 2 diameters embedded in a homogeneous soil characterized by a shear wave velocity of 100 m/s, while the case C_4E_250 indicates a reinforced concrete caisson of length equal to 4 diameters embedded in a non-homogeneous soil deposit characterized by a shear wave velocity of 250 m/s at depth of one pile diameter. Some parameters, deemed to have a minor effect on the variability of impedances and on the kinematic response [32], are assumed to be constant; in detail, a density $\rho_s = 2.0$ t/m^3 and a Poisson's ratio $\nu_s = 0.4$ are considered for the soil. As for caissons, densities ρ_c equal to 2.5 and 7.85 t/m^3, and Poisson's ratios ν_c equal to 0.2 and 0.3 are considered for reinforced concrete and the steel skirts, respectively.

By defining the non-dimensional frequency $a_0 = \omega D/V_{s,D}$, analyses are performed within the frequency range 0÷6, which covers, for all the investigated cases, the frequency range of interest for engineering applications (0÷10 Hz). The lid mass is not considered, consistently with a conventional application of the substructure approach. Finally, in order to make applications repeatable by a reader and for the sake of completeness, analyses are performed considering an elastic modulus *E* for the caisson material of 30 and 210 GPa for the concrete and the steel, respectively. By defining with E_s the elastic modulus of the soil, the latter generate an E/E_s ratio ranging between 536 and 86 for the concrete caissons and between 3750 and 600 for the steel caissons.

Firstly, an overview of the overall performance of the proposed model is presented by defining an error parameter to quantify discrepancies with respect to the benchmark model's results in terms of frequency-dependent impedances and kinematic response factors; then, starting from the information obtained from the overall errors, selected results of some specific configurations are shown to illustrate the performance of the model and to provide a visual correlation between the error parameter and the model behaviour.

3.3 Overview of the overall errors

In order to provide an overview of the discrepancies between the results obtained from the proposed model and the benchmark, the following overall error parameters are defined in the investigated frequency range to quantify differences between the two functions (frequency-dependent impedances and kinematic response factors):

$$\varepsilon_i = 1 - \phi_i \tag{32}$$

where

$$\phi_i = \frac{\int_0^{f_{up}} \blacksquare_i^m(f)\,\blacksquare_i^b(f)\,df}{\int_0^{f_{up}} \left(\blacksquare_i^b(f)\right)^2 df} \tag{33}$$

In Equation (33), subscript *i* identifies the generic quantity for which the parameter is computed, *f* is the frequency, ■ is the generic component of the impedance matrix or one of the kinematic response factors, and superscripts *m* and *b* identify results obtained from the model and the benchmark results, respectively. Parameters ϕ are 1 if the generic quantity obtained from the model superimpose to the relevant one of the benchmark data; thus, the error parameters ε tends to 0 by reducing differences between the computed quantities and the benchmark data. The error parameters are computed considering different values of the upper bound of the integral f; in detail, 2, 5 and 10 Hz are considered. It is worth noting that the parameters are referred to the dimensional frequency ranges to make the overview of the model accuracy directly comparable with the frequency content of an earthquake or the fundamental frequency of the superstructure.

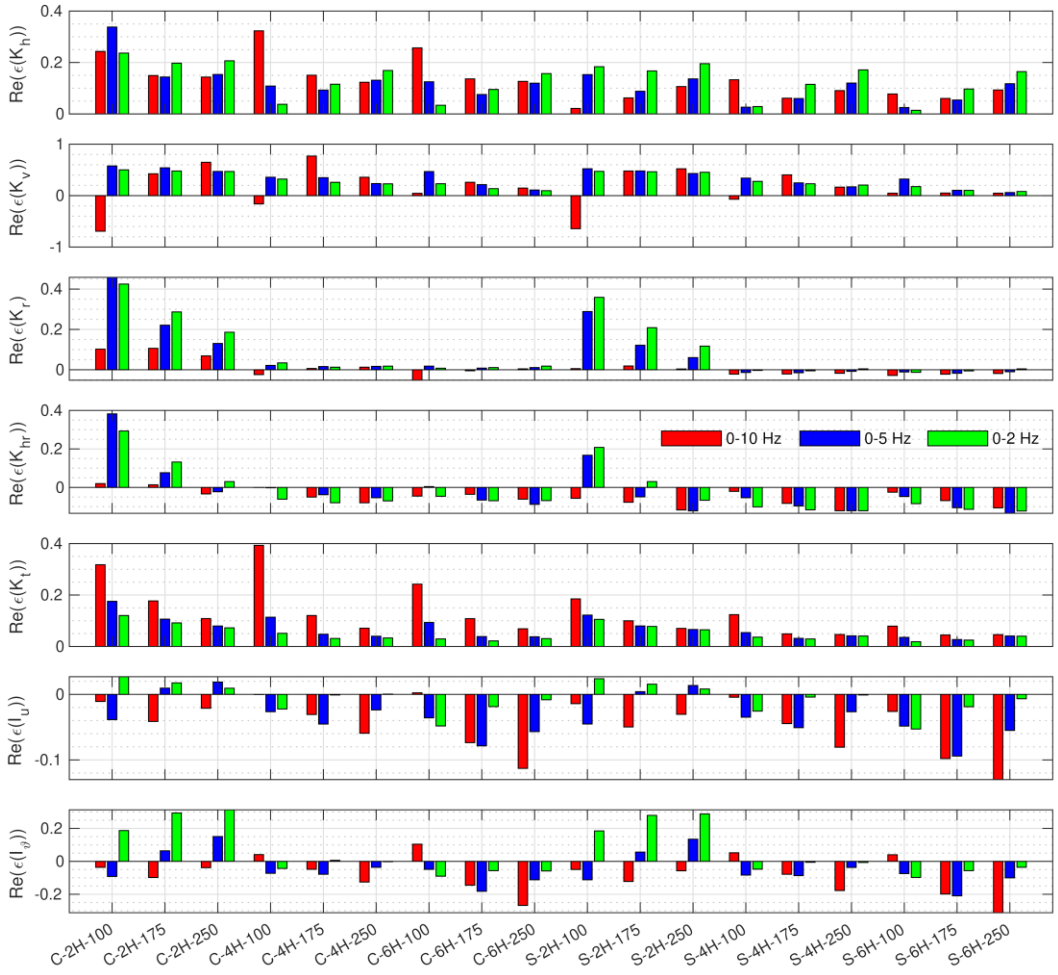

Figure 6. Errors computed for the real parts of all impedance and FIM components. Homogeneous (H) profile. BEM-FEM model without lid.

In order to illustrate how the distribution of errors vary among the different configurations, Figures 6 and 7 present the ε value computed for the real and imaginary parts, respectively, of all impedance functions and both kinematic factors for all the foundation cases in the homogenous profile without including the lid in the BEM-FEM model used as reference.

It can be remarked that very low values of the error parameters are obtained for all the real parts of the impedance functions and the kinematic response functions; in detail, parameters are all below 0.4 for the translational, rotational, coupled roto-translational and torsional impedances, with a great number of cases presenting values lower than 0.2. In addition, the rotational and coupled-roto translational components show a very good matching with the benchmark data, as documented by a numerous set of cases characterised by an error parameter below 0.1. Slightly higher values of the errors are obtained for the real parts of the vertical impedance, while the kinematic response parameters are well captured, with errors almost always below 0.2. As for imaginary parts, slightly higher values of the errors can be observed; anyway, errors are always below 0.5-1.0 for impedances while sensibly higher parameters can be observed for the imaginary parts of the kinematic

response factors. The latter are due to peculiar trends of the results with frequency that will be commented in the sequel with respect to some selected case studies.

The distribution of errors for the non-homogeneous soil profile (E) follows, in general, the same trends, although average differences are higher, and large differences can be found for some individual cases. The same can be said if the results from the proposed model are compared against the benchmark model that considers the presence of the lid in contact with the ground surface, case in which differences are larger (these results are not shown here for the sake of brevity). These distributions of errors are synthesized below in order to show the main trends more clearly.

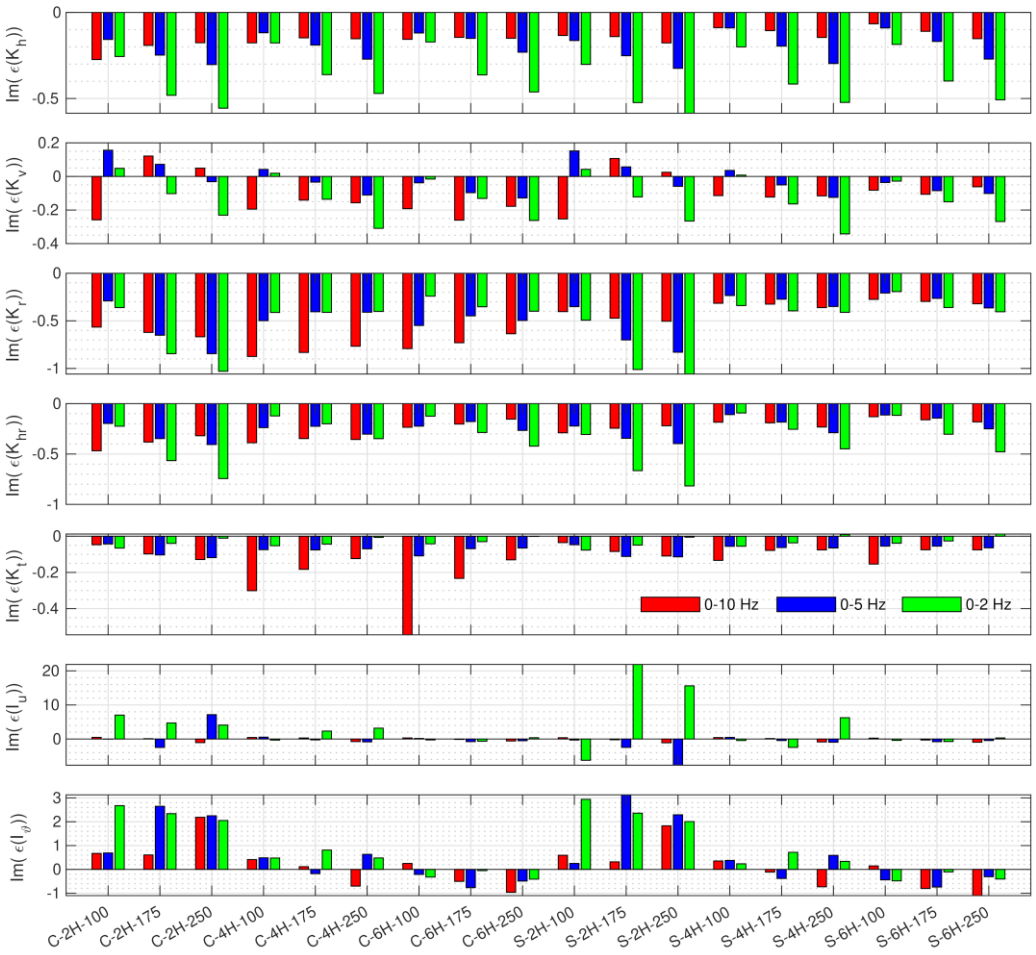

Figure 7. Errors computed for the imaginary parts of all impedance and FIM components. Homogeneous (H) profile. BEM-FEM model without lid.

In order to determine more clearly how the accuracy and applicability of the proposed Winkler model is affected by the different parameters, Figures 8 and 9 present a statistical analysis of the errors. Each box plot presents the median, 25th and 75th percentiles and the nonoutlier minima and maxima of the absolute values of all errors relevant to the indicated case. For instance, the first box plot (corresponding to $V_{s,D}$ = 100 m/s) of the first plot, is computed using all the errors corresponding to all cases with such representative shear wave velocity, i.e., it is representative of 84 individual cases (7 response quantities, i.e. 5 impedance functions and 2 kinematic response factors, times 3 slenderness ratios times 2 materials times 2 profiles). Furthermore, the statistical analysis is performed considering values of errors obtained within two frequency ranges, 0-2 Hz and 0-10 Hz; these have been selected considering the application fields of caisson foundations (e.g. OWTs and bridges) and taking into account the seismic problem. Indeed, for particularly slender cantilever structures, such as OWTs, the seismic response is largely dominated by the first fundamental frequency, usually lower than 2 Hz; on the other hand, for structures characterised by a more complex response, such as bridges, the frequency range of interest is usually limited to 0-10 Hz, where the earthquakes have the highest energy content and the resonance frequencies of the structure fall.

Figure 8 analyses the errors computed with respect to the BEM-FEM model that does not include the lid, while Figure 9 reports the errors with respect to the BEM-FEM model that considers the presence of the lid. As previously observed, real parts of all the response quantities are characterised by lower errors with respect to the imaginary parts.

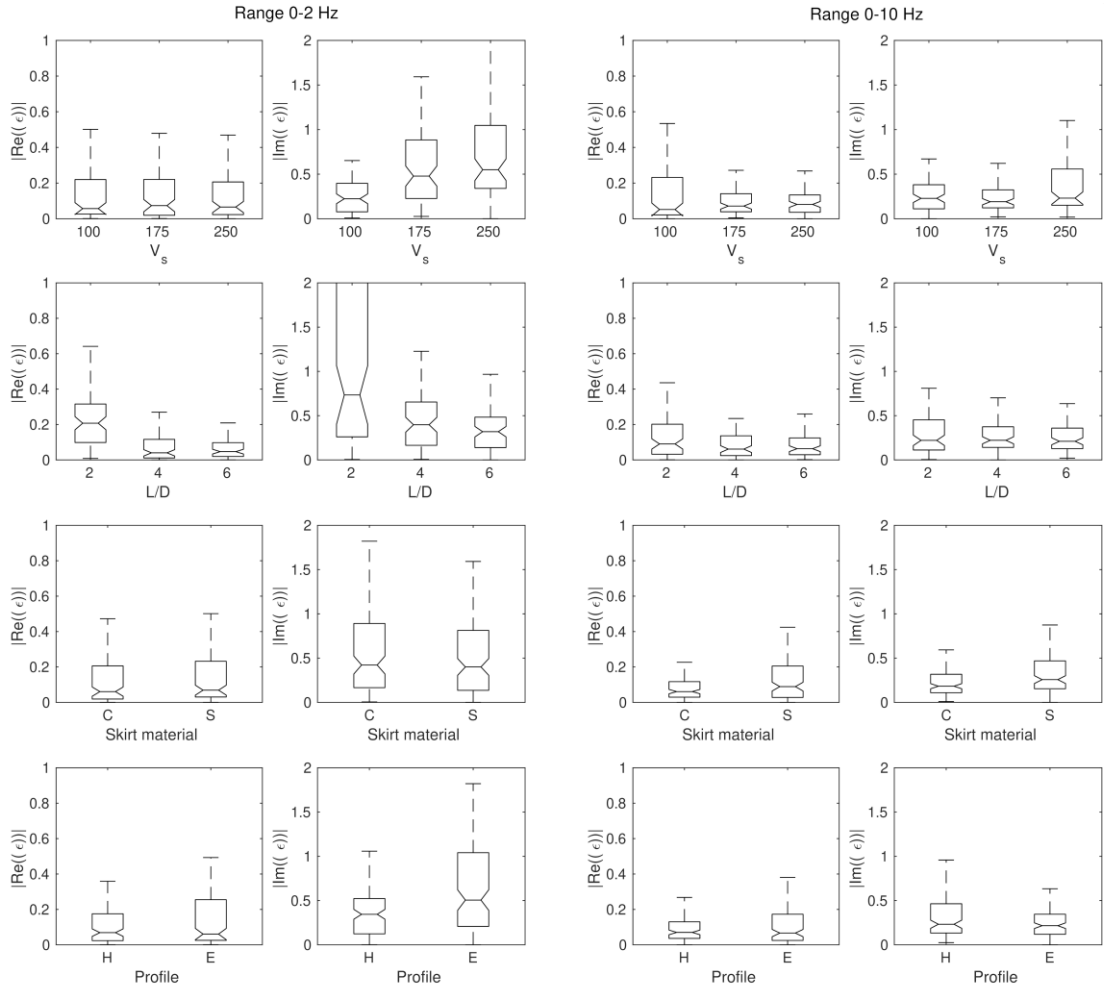

Figure 8. Evolution of errors with respect to shear wave velocity, slenderness ratio, skirt material and soil profile. On the left, errors computed from differences in the range 0-2 Hz. On the right, errors computed from differences in the range 0-10 Hz. Outliers are not plotted. Benchmark results from the BEM-FEM model are computed without lid.

As for real parts, the accuracy of the model is almost independent on the shear wave velocity in the range 0-2 Hz, while it increases if the range 0-10 is considered. Furthermore, for both frequency ranges, an increase of the model accuracy is observed by increasing the slenderness ratio. In addition, slightly better results are obtained for concrete foundations in homogeneous profiles, both in the 0-2 and 0-10 Hz frequency ranges. Concerning imaginary parts, the model accuracy worsens by increasing the shear wave velocity (especially in the range 0-2 Hz) while it still increases with the slenderness ratio (as before, the accuracy increment is more evident in the range 0-2 Hz). Finally, considerations similar to those of the real parts hold for what concerns the error dependency on the skirt material and the soil profile. Comparing data obtained for the two frequency ranges, it appears evident that discrepancies between results of the proposed model and the benchmarks are frequency-dependent; higher errors are obtained for low frequency ranges, as a consequence of the intrinsic drawbacks of the adopted expressions for the soil reactions, which, as already stated, collapse for $\omega \to 0$, and for which the correction proposed in [45] has been adopted.

Comparing data from the two figures, it is clear that greater errors are obtained if the lid is considered in computing results from the BEM-FEM model.

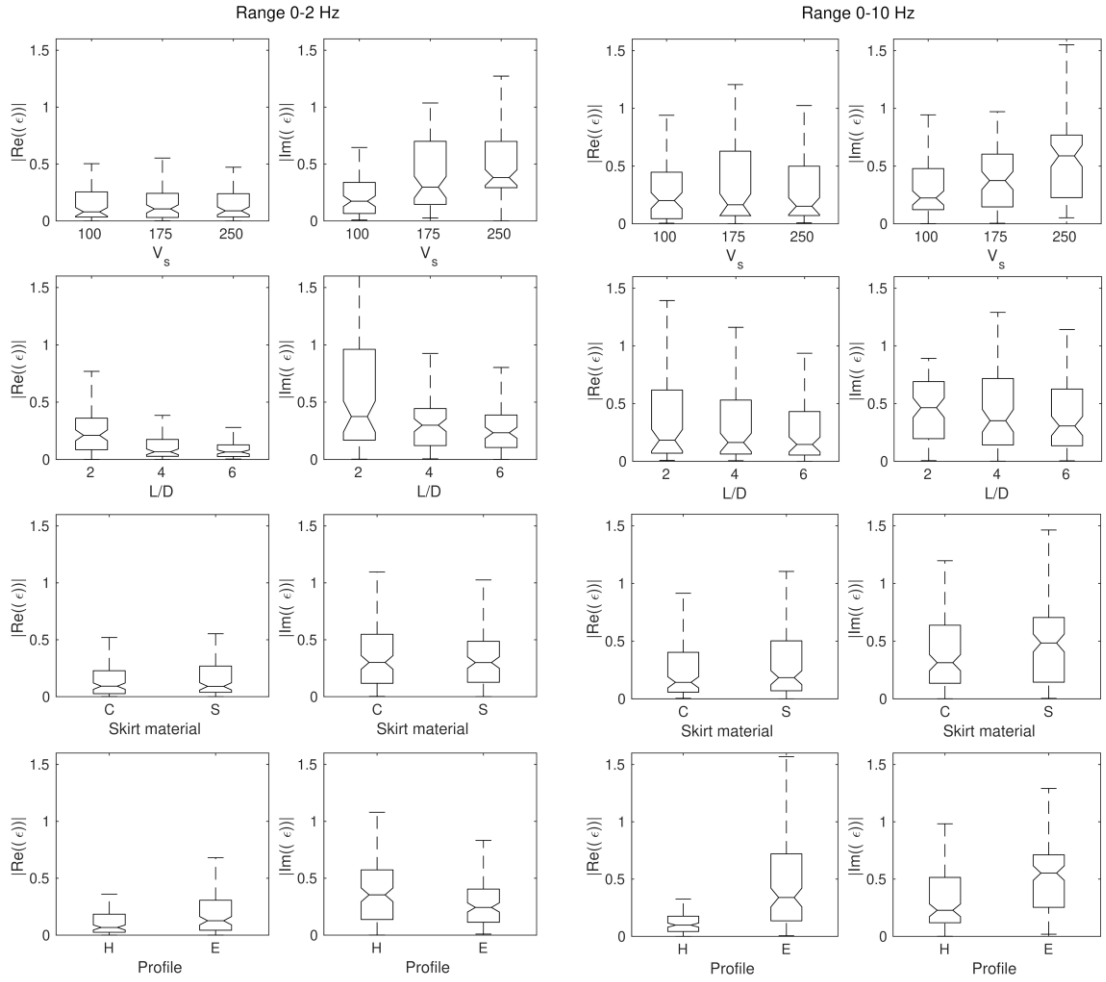

Figure 9. Evolution of errors with respect to shear wave velocity, slenderness ratio, skirt material and soil profile. On the left, errors computed from differences in the range 0-2 Hz. On the right, errors computed from differences in the range 0-10 Hz. Outliers are not plotted. Benchmark results from the BEM-FEM model are computed with lid.

3.4 Impedance functions and kinematic response

According to Figures 8 and 9, it can be said that the configuration for which the proposed Winkler model reaches, in average, a higher level of agreement with respect to the reference BEM-FEM model is for a concrete foundation with a slenderness ratio L/D = 6, embedded in a homogenous profile with $V_{s,D}$ = 250 m/s. On the contrary, the worst agreement is found for the case of a steel foundation with a slenderness ratio L/D=2, embedded in the non-homogenous profile with $V_{s,D}$ = 100 m/s. In order to facilitate the reader to correlate the error parameters with the actual discrepancies of the model results with the benchmark data, differences found in all individual functions (i.e., the impedances and kinematic interaction factors) are illustrated for these two representative cases. In addition, results obtained from a Winkler model implementing the closed-form expressions obtained by Novak from the plane strain solution of an infinitely long cylinder [43] are added. For these applications, the soil inside the caissons is considered to contribute in terms of mass and inertia through a simple homogenization of the cross-sections. Comparisons of results obtained from the proposed model with the latter applications provide a clear overview of the role of the interactions arising between the caisson and the soil inside.

Figures 10 and 11 present the comparisons between the impedance functions yielded by the proposed Winkler model (red continuous lines) and the reference BEM-FEM model including the lid or not (black continuous and dashed lines, respectively), for the two representative cases mentioned above. In the same plots, results obtained from the Winkler model implementing only the Novak's closed-form expressions for the external soil reactions are shown with dashed red lines. As for Figure 10, relevant to a slender concrete caisson in homogeneous soil profile of medium stiffness, a good matching between the impedances obtained from the proposed model and the benchmark data, disregarding the lid, are obtained, except for the torsional impedance. In addition, it is worth noting the model capability in capturing the peak of maximum impedance of the soil-caisson system. On the contrary, the benchmark impedances obtained by considering the lid are sensibly different from those obtained with the proposed model. Overall, peaks occur at lower frequencies and become evident in the selected non-dimensional frequency range also for the translational, rotational and coupled roto-

translational terms of impedances; the latter are not captured by the proposed model. The soil-caisson interactions triggered by the internal soil do not affect sensibly the impedance components, excepting for the vertical one, for which the soil vibrating inside the caisson produces peaks that cannot be captured by disregarding the stiffness of the internal soil.

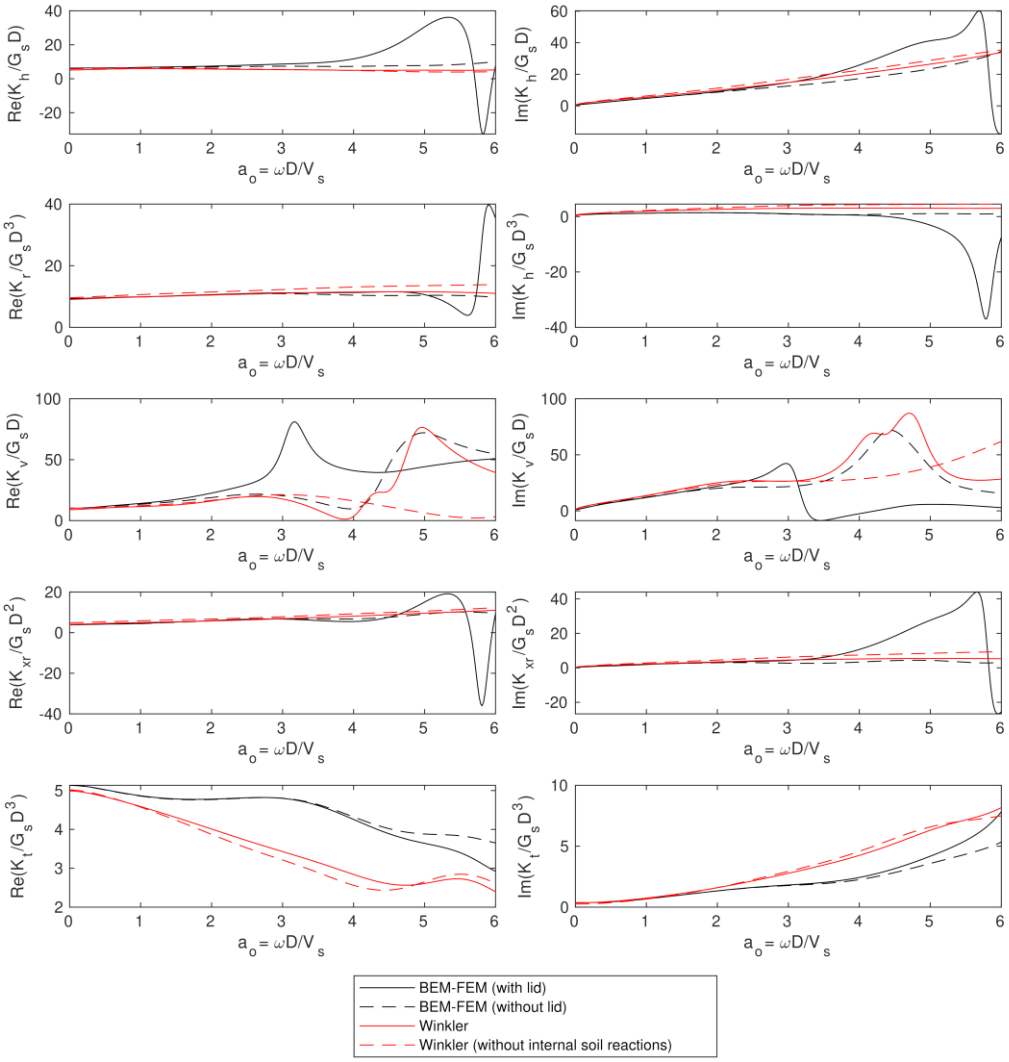

Figure 10. Comparison between impedance functions: concrete foundation, homogenous soil, L/D=6, $V_{s,D}$=250 m/s.

Concerning Figure 11, referred to a steel caisson with a low slenderness ratio in a non-homogenous loose soil deposit, an overall capability of the proposed model in capturing the impedance functions can be observed up to a non-dimensional frequency of about 3.5. For higher frequencies, peaks of impedances highlighted by the reference BEM-FEM model, with or without the lid contribution, cannot be captured by the proposed model. In addition, the comparison between the responses provided by the Winkler models that consider, or neglect, the internal soil reactions (solid and dashed red curves) highlights the relevance of the contribution of the soil inside the caisson in all the terms of the impedance matrix, being the proposed model (that includes the internal soil reactions) more prone to reproduce the reference BEM-FEM results (particularly for the rotational and coupled roto-translational terms).

As already shown by Liingaard et al. [24], and by the present results from the reference BEM-FEM model, the lid has an important impact on all impedance components except the torsional one. This strong influence is explained by the fact that the lid imposes a kinematic constraint to the soil surface, whereas the soil surface is traction-free when no lid is considered. The corresponding soil reaction at the lid triggers a complex three-dimensional wave field inside the caisson. Signs of this are captured by the relevant impedance components where peaks presumably related to modes of vibration of the internal soil appear. The present proposed Winkler model includes only the part of the physical phenomena related to the two-dimensional plane strain soil-skirt interaction. This is quite evident when comparing the peaks in the vertical impedances from all the models considered. Including soil-lid interaction in the present Winkler model is not a straightforward matter since there is a strong interdependence between soil-lid reaction and soil-skirt reaction, leading to a fully three-dimensional phenomenon. Thus, approaches such as using a single spring-dashpot with the impedance of a

surface foundation for modelling the lid do not work. Probably, a Winkler model including soil-lid interaction would require depth-dependent soil reactions, which very likely ban the main two advantages of Winkler models: simple formulation and low computational cost. Therefore, the present proposed Winkler model is able to represent physical situations where the lid (if present) has a small influence over the response.

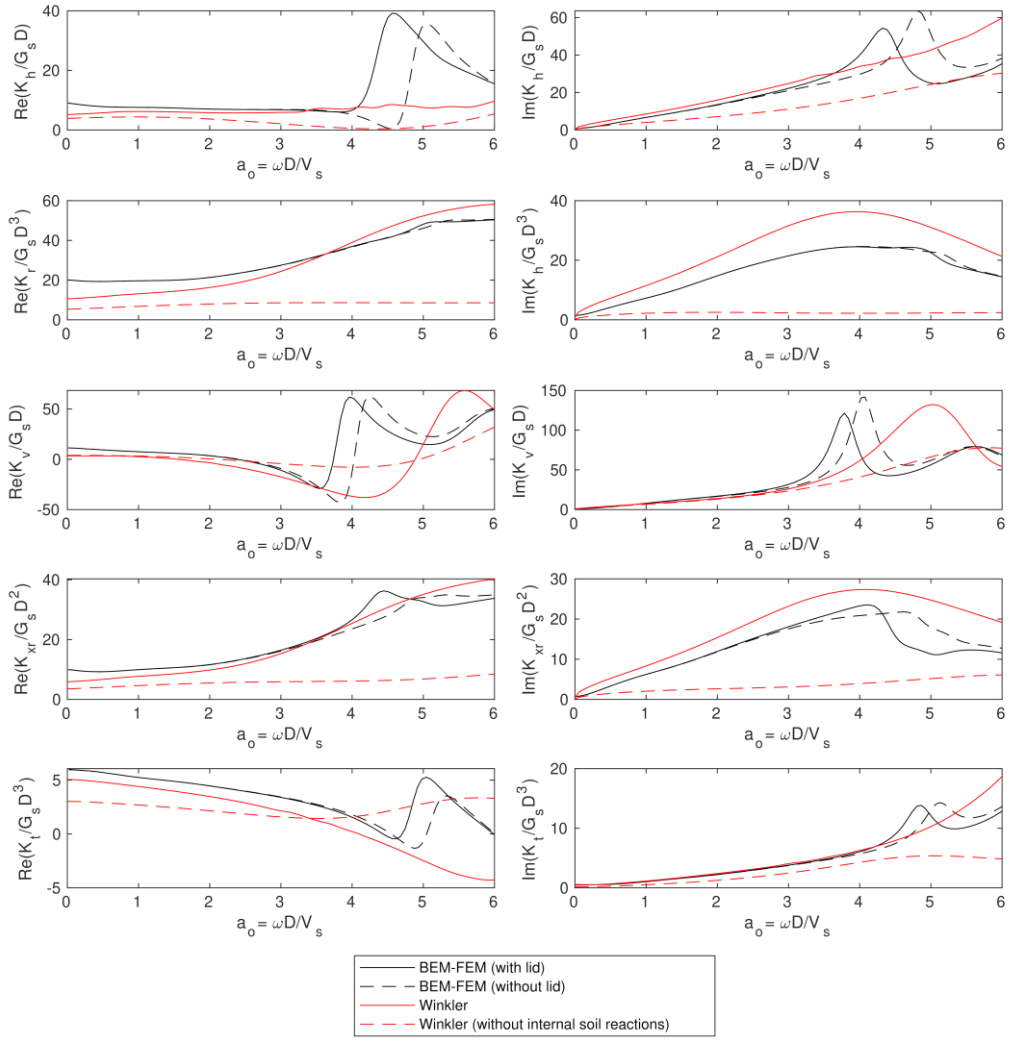

Figure 11. Comparison between impedance functions: steel foundation, non-homogenous soil, L/D = 2, $V_{s,D}$ = 100 m/s.

Figures 12 and 13 present the comparisons between the kinematic interaction factors

$$\mathrm{I_u} = \frac{u_i}{u_{i,ff}} \tag{34a}$$

$$\mathrm{I_\phi} = \frac{\varphi_i}{u_{i,ff}} \tag{34b}$$

computed with the proposed Winkler model and the reference BEM-FEM model including the lid or not, for the same two cases. In Equation (34a,b) u_i and $u_{i,ff}$ are the pile head and the free-field displacements in the i-th direction, respectively, while φ_i is the pile head rotation around the i-th axis. Also in this case, results obtained by using only Novak's expressions are reported for comparison. For both the selected case studies, a very good matching is observed concerning the real parts of the functions while important discrepancies can be noted, especially for the slender concrete caisson, for the imaginary parts, consistently with results presented in the previous sections. Interactions arising between the caissons and the internal soil largely affect the imaginary components of the kinematic response parameters while a less evident impact is observed in the real parts. Unlike impedances, kinematic interaction factors are quite unaffected by soil-lid interaction. Therefore, for all the presented cases, the proposed Winkler model behaves better than that implementing only the Novak's expressions.

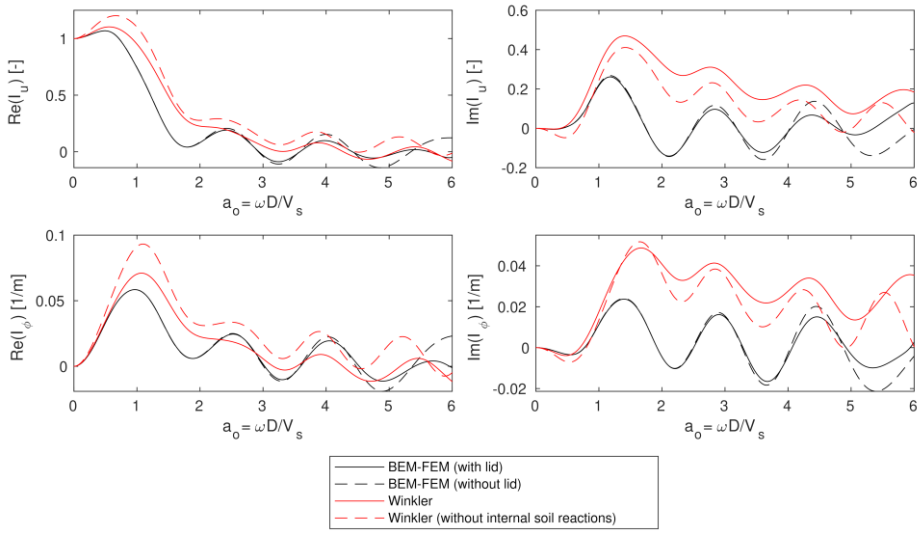

Figure 12. Comparison between kin. interaction factors: concrete foundation, homogenous soil, L/D=6, $V_{s,D}$=250 m/s.

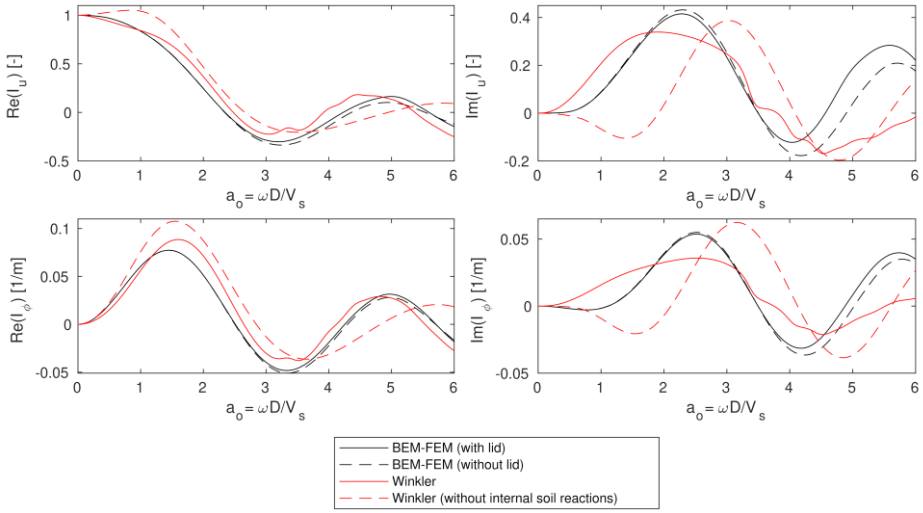

Figure 13. Comparison between kin. inter. factors: steel foundation, non-homogenous soil, L/D = 2, $V_{s,D}$ = 100 m/s.

4 ACCURACY OF THE SEISMIC RESPONSE PREDICTION

The accuracy of the proposed model in capturing the seismic response of real caisson foundations (e.g. displacements, accelerations and stress resultants) is studied in this section considering foundations of real OWTs. In detail, foundations of the NREL 5MW [33], the IEA-10.0-198-RWT [34], and the IEA-15-240-RWT [35] reference wind turbines are considered and subjected to 3 real earthquakes characterized by different intensities and frequency content. The adopted accelerograms, taken from the European Strong Motion Database [36], are detailed in Table 2. Figure 14 shows the time histories and the Fourier amplitude spectra of the strong-motion of each registration, which is applied at the surface of the soil deposit; it is worth observing the different frequency content of the selected earthquakes (up to 10 Hz) that makes it possible to investigate the ability of the proposed approach in capturing displacements, accelerations and stress resultants on caissons taking into account the different performance of the model with the frequency of the input excitation (as demonstrated in previous sections). The properties of the considered OWT caisson foundations are shown in Table 3.

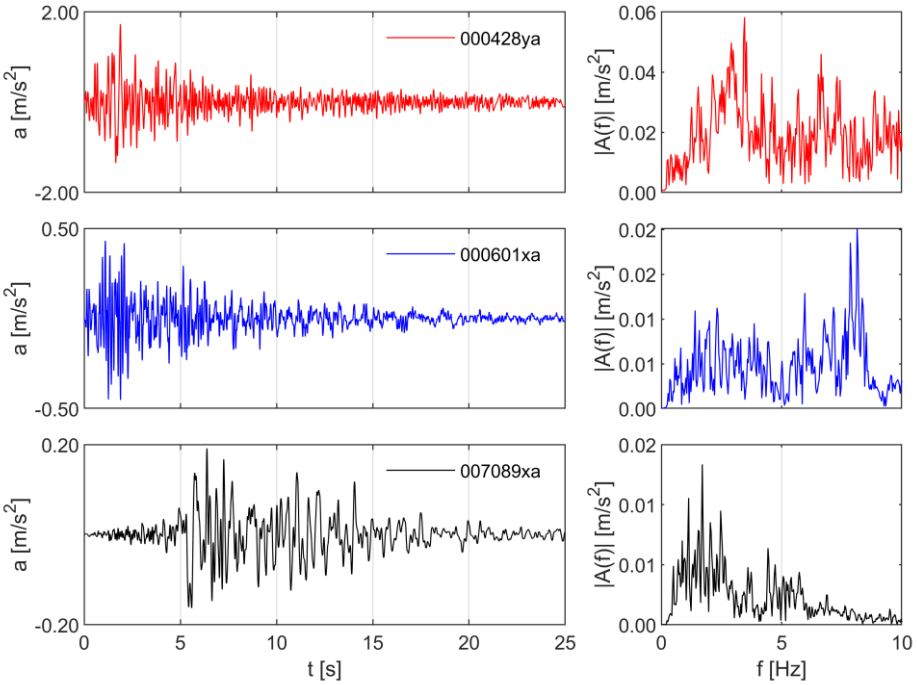

Figure 14. Time histories and Fourier Amplitude Spectra of the three selected accelerograms.

Table 2: Selected real earthquakes

Earthquake Name	**Wave form ID**	**Country**	**Station ID**	**Date** [dd/mm/yy]	**Δ** [km]	**Magnitude** [M_w]	**PGA** [m/s^2]
Etolia	428ya	Greece	ST169	18.05.1988	23	5.3	1.730
Umbria-Marche	601xa	Italy	ST224	26.09.1997	27	5.7	0.452
Pasinler	7089xa	Turkey	ST557	10.07.2001	32	5.4	0.192

Table 3: Geometry of caissons and dynamic properties of the soil deposits

	NREL 5MW	**IEA-10.0-198-RWT**	**IEA-15-240-RWT**
Caisson diameter (D) [m]	6	9	10
Skirt thickness (s) [mm]	60	101.5	55.3
Pile depth (L) [m]	36	42.6	45
L/D	6	4.73	4.5
Young's modulus, E_c [GPa]	210	210	200
Shear modulus, G_c [GPa]	80.8	80.8	79.3
Density ρ_c [t/m^3]	8.5	8.5	7.85
Soil profile	Layered	Single layer	Single layer
Soil type	Sand	Sand	Dense sand or Gravel
Soil Poisson's ratio ν_s [-]	0.35	0.3	0.4
Density ρ_s [t/m^3]	2	2	2
Shear modulus G_s [GPa]	42.6 ($0 < z < 5$ m) 61.9 ($5 < z < 14$ m) 87.4 ($14 < z < \infty$)	92.3 ($0 < z < \infty$)	140 ($0 < z < \infty$)
Shear wave velocity V_s [m/s]	145.9 ($0 < z < 5$ m) 175.9 ($5 < z < 14$ m) 209 ($14 < z < \infty$)	214.8 ($0 < z < \infty$)	264.5 ($0 < z < \infty$)
Soil damping ratio ξ_s [-]	0.05	0.05	0.05

Figure 15 shows the non-null components of the impedance matrix of the caissons foundations of the three OWTs. Continuous lines refer to data obtained with the proposed approach while dashed lines are used for the benchmark data (the contribution of the lid is considered), provided by the BEM-FEM model. In addition, for the generic component, real

and imaginary parts are reported in the same graph with red and blue lines, respectively. It can be observed that all impedances are closely reproduced in the frequency range 0-10 Hz, particularly the rotational, torsional and coupled roto-translational terms. Translational and vertical components present some discrepancies in the range 0-2 Hz while are very good captured for higher frequency ranges.

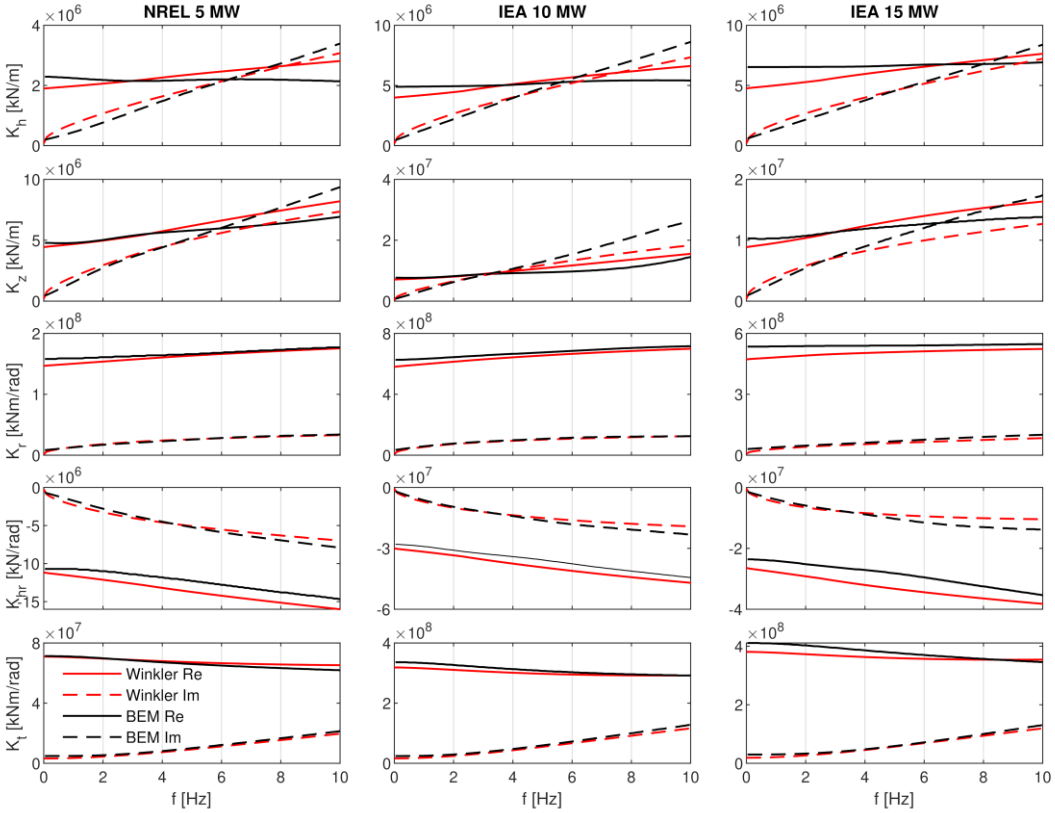

Figure 15. Computed impedances for the three foundations.

Figure 16 presents the kinematic response factors of the three foundations by adopting the same representative rules; the kinematic response obtained from the proposed model is sensibly different from that obtained from the BEM-FEM model (including the lid contribution), especially for what concern the imaginary parts. The response that is approximated better is that of the 10MW OWT for which the real parts of both the translational and rotational kinematic response factors obtained from the BEM-FEM model is very well captured.

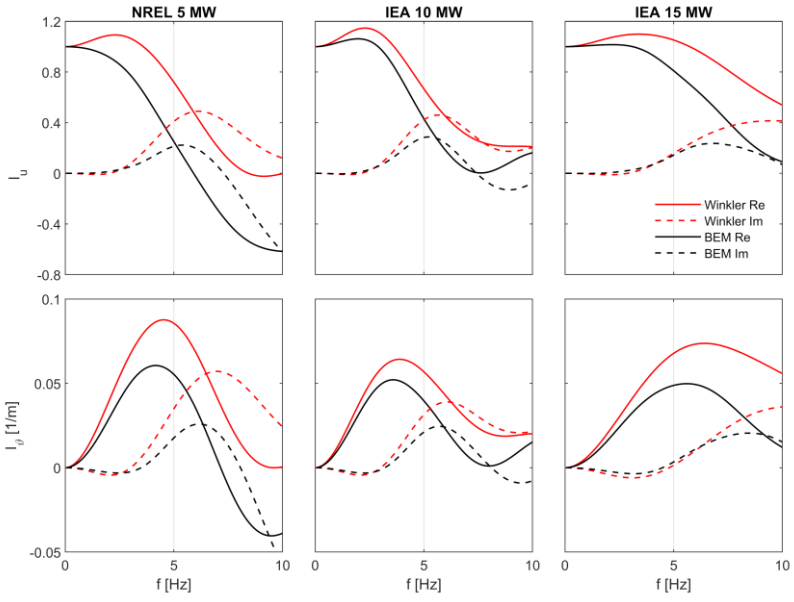

Figure 16. Computed kinematic response factor for the three foundations.

Figure 17 shows the time histories of the caissons head displacements and rotations obtained for the three earthquakes; these correspond to the foundation input motion and constitute the input to the superstructure in the framework of soil-structure interaction analyses performed in the spirit of the substructure approach. The selected accelerograms are assumed to be applied at the soil surface. Despite discrepancies observed in Figure 16 between the kinematic response factors computed with the proposed model and with the BEM-FEM one, caisson head displacements and rotations superimpose with a very good accuracy, even if the peak rotations are slightly underestimated by the proposed model.

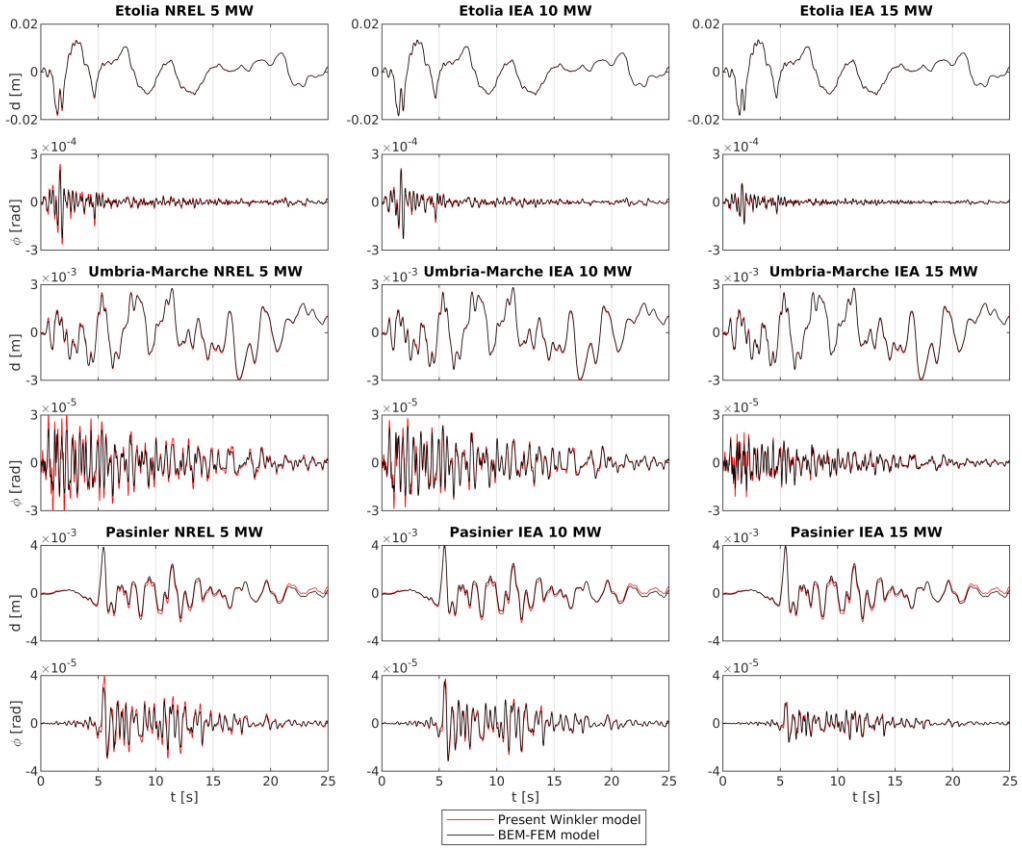

Figure 17. Comparison between time-history responses in terms of caisson head displacements and rotations.

Finally, Figure 18 shows the maximum and minimum envelops of the kinematic stress resultants along the caissons due to the propagation of the seismic shear waves inside the deposits. The proposed model accurately reproduces results of the BEM-FEM model with some minor differences relevant to shear forces at the caisson base.

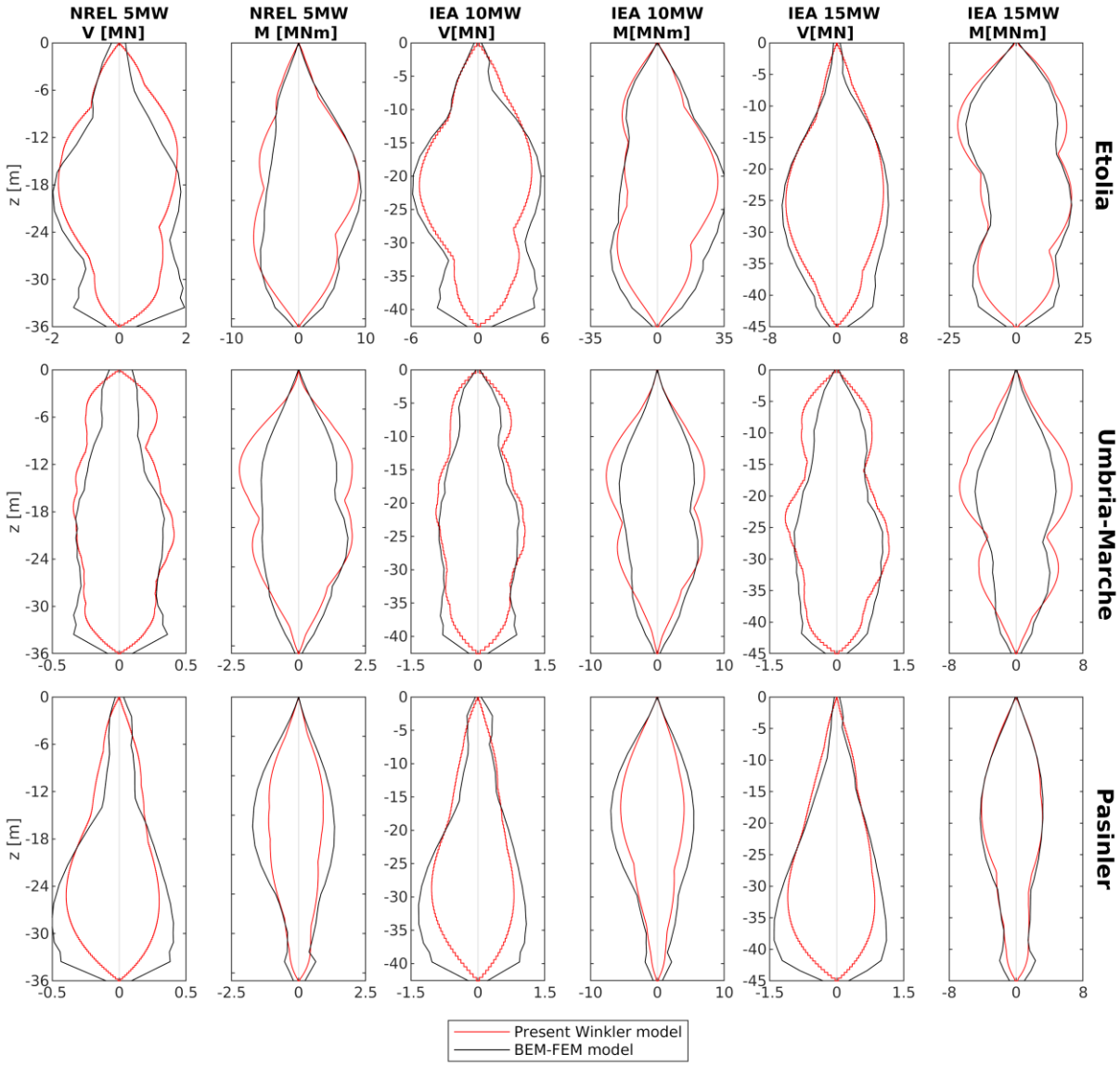

Figure 18. Comparison between envelopes of kinematic shear forces and bending moments.

5 CONCLUSIONS

A Winkler-based numerical model for the analysis of the dynamic response of caissons foundations has been presented in this paper. A Timoshenko beam model is used for the caisson and the soil-caisson interactions are introduced through functions expressing the soil reactions as a function of the relative displacements between the soil and the caisson. Winkler models usually consider only the reactions of the soil outside the foundation. In this case, the reactions from the soil inside the foundation are also included. Specific functions are derived to this end using the same approach and simplifying initial assumptions used to obtain the widely used Novak's expressions for the reactions of the soil outside a pile. The problem is solved numerically through a finite element approach. The model capabilities in capturing the dynamic response of a wide set of concrete and steel caisson foundations embedded in homogeneous and non-homogeneous soil deposits are investigated through comparisons with data obtained by a rigorous BEM-FEM model.

The following main conclusions can be drawn:

- the model is characterised by few degrees of freedom since the soil is not physically included in the formulation and the solution is characterised by a very low computational demand;
- the consideration of the reactions of the soil within the foundation contributes to significantly improve the accuracy of the solution for this type of problems.
- the model capability in capturing impedances and kinematic response factors of caisson foundations obtained through more rigorous approaches is quite good; accuracy in predicting the real parts of the response quantities increases by increasing the shear wave velocity of the soil and the slenderness ratio of the caisson; on the contrary, the accuracy of the imaginary parts decrease by increasing the shear wave velocity and are overall characterised by a lower degree of precision with respect to the real parts;
- the model seems to provide better results in case of homogeneous soil deposits;

- despite discrepancies observed with results of rigorous approaches in terms of impedances and kinematic response factors, applications to realistic caisson foundations subjected to real earthquakes demonstrate that the model is able to predict very well the foundation input motion and the maximum stress resultants arising along the shaft due to the propagation of the seismic waves;
- overall, the model behaves better than a Winkler one in which the soil inside the caisson only contributed in term of mass and inertia propertied (through a cross-section homogenization) and in which the soil interactions with the external soil are captured exploiting the Novak's closed-form expressions.

In conclusion, the proposed model revealed suitable for applications in realistic engineering contexts, and, in view of its low computational effort, it is a versatile tool for large scale phenomenological or probabilistic investigations on the kinematic response of caisson foundations in homogeneous or stratified media.

ACKNOWLEDGMENTS
This work is part of the research project PID2020-120102RB-I00 funded by MCIN/AEI/10.13039/501100011033.

REFERENCES
[1] EWEA, Offshore Wind in Europe - Key trends and statistics 2019, Wind Europe, 2020.
[2] Chaudhary, M. T. A., Abe, M., & Fujino, Y. (2001). Identification of soil–structure interaction effect in base-isolated bridges from earthquake records. Soil Dynamics and Earthquake Engineering, 21(8), 713-725.
[3] Sextos, A. G., Kappos, A. J., & Pitilakis, K. D. (2003). Inelastic dynamic analysis of RC bridges accounting for spatial variability of ground motion, site effects and soil–structure interaction phenomena. Part 2: Parametric study. Earthquake Engineering & Structural Dynamics, 32(4), 629-652.
[4] Mylonakis, G., Nikolaou, S., & Gazetas, G. (2006). Footings under seismic loading: Analysis and design issues with emphasis on bridge foundations. Soil Dynamics and Earthquake Engineering, 26(9), 824-853.
[5] Carbonari, S., Dezi, F., & Leoni, G. (2011). Seismic soil–structure interaction in multi-span bridges: Application to a railway bridge. Earthquake engineering & structural dynamics, 40(11), 1219-1239.
[6] Dezi, F., Carbonari, S., Tombari, A., & Leoni, G. (2012) Soil-structure interaction in the seismic response of an isolated three span motorway overcrossing founded on piles. Soil Dynamics and Earthquake Engineering, 41:151-163.
[7] González, F., Padrón, L. A., Carbonari, S., Morici, M., Aznárez, J. J., Dezi, F., & Leoni, G. (2019). Seismic response of bridge piers on pile groups for different soil damping models and lumped parameter representations of the foundation. Earthquake Engineering & Structural Dynamics, 48(3), 306-327.
[8] DNV. Guidelines for design of Wind Turbines. 2nd ed. Det Norske Veritas, Copenhagen and Wind Energy Department, Risø National Laboratory, 2002.
[9] Kühn, M. J. (2001). Dynamics and design optimisation of offshore wind energy conversion systems. DUWIND, Delft University Wind Energy Research Institute.
[10] Van Der Tempel, J. (2006). Design of support structures for offshore wind turbines.
[11] Wang, L., & Dong, X. T. (2011). Influence of earthquake directions on wind turbine tower under seismic action. In Advanced Materials Research (Vol. 243, pp. 3883-3888). Trans Tech Publications Ltd.
[12] Stamatopoulos, G. N. (2013). Response of a wind turbine subjected to near-fault excitation and comparison with the Greek Aseismic Code provisions. Soil Dynamics and Earthquake Engineering, 46, 77-84.
[13] Díaz, O., & Suárez, L. E. (2014). Seismic analysis of wind turbines. Earthquake Spectra, 30(2), 743-765.
[14] Asareh, M. A., Schonberg, W., & Volz, J. (2016). Effects of seismic and aerodynamic load interaction on structural dynamic response of multi-megawatt utility scale horizontal axis wind turbines. Renewable energy, 86, 49-58.
[15] De Risi, R., Bhattacharya, S., & Goda, K. (2018). Seismic performance assessment of monopile-supported offshore wind turbines using unscaled natural earthquake records. Soil Dynamics and Earthquake Engineering, 109, 154-172.
[16] Ali, A., De Risi, R., Sextos, A., Goda, K., & Chang, Z. (2020). Seismic vulnerability of offshore wind turbines to pulse and non-pulse records. Earthquake Engineering & Structural Dynamics, 49(1), 24-50.
[17] Wolf J.P. (1988). Soil-Structure-Interaction Analysis in Time Domain. Pearson College Div. ISBN 10: 0138229740
[18] Beredugo, Y. O., & Novak, M. (1972). Coupled horizontal and rocking vibration of embedded footings. Canadian Geotechnical Journal, 9(4), 477-497.
[19] Veletsos, A. S., & Younan, A. H. (1995). Dynamic modeling and response of rigid embedded cylinders. Journal of Engineering Mechanics, 121(9), 1026-1035.
[20] Saitoh, M., & Watanabe, H. (2004). Effects of flexibility on rocking impedance of deeply embedded foundation. Journal of geotechnical and geoenvironmental engineering, 130(4), 438-445.
[21] Gerolymos, N., & Gazetas, G. (2006). Static and dynamic response of massive caisson foundations with soil and interface nonlinearities—validation and results. Soil Dynamics and Earthquake Engineering, 26(5), 377-394.
[22] Gerolymos, N., & Gazetas, G. (2006). Development of Winkler model for static and dynamic response of caisson foundations with soil and interface nonlinearities. Soil Dynamics and Earthquake Engineering, 26(5), 363-376.
[23] Beltrami, C., Lai, C. G., & Pecker, A. (2005). A kinematic interaction model for a large-diameter shaft foundation: An application to seismic demand assessment of a bridge subject to coupled swaying-rocking excitation. Journal of Earthquake Engineering, 9(spec02), 355-393.
[24] Liingaard, Andersen & Ibsen (2007) Impedance of flexible suction caissons. Earthq Eng Struct Dyn, 36, 2249-2271.
[25] Latini, C., & Zania, V. (2017). Dynamic lateral response of suction caissons. Soil Dyn Earthq Eng, 100, 59-71.

[26] Jalbi, S., Shadlou, M., & Bhattacharya, S. (2018). Impedance functions for rigid skirted caissons supporting offshore wind turbines. Ocean Engineering, 150, 21-35.
[27] Lian, J., Jiang, Q., Dong, X., Zhao, Y., & Zhao, H. (2019). Dynamic Impedance of the Wide-Shallow Bucket Foundation for Offshore Wind Turbine Using Coupled Finite–Infinite Element Method. Energies, 12(22), 4370.
[28] Skau, K. S., Jostad, H. P., Eiksund, G., & Sturm, H. (2019). Modelling of soil-structure-interaction for flexible caissons for offshore wind turbines. Ocean Engineering, 171, 273-285.
[29] Latini, C., & Zania, V. (2019). Vertical dynamic impedance of suction caisson. Soils and Foundations, 59 1113-1127.
[30] Kuhlemeyer, R. L., & Lysmer, J. (1973). Finite element method accuracy for wave propagation problems. Journal of the Soil Mechanics and Foundations Division, 99(5), 421-427.
[31] Bordón, J.D.R., Aznárez, J.J. & Maeso O. (2017). Dynamic model of open shell structures buried in poroelastic soils. Computational Mechanics, 60(2):269–288.
[32] Minnucci, L., Morici, M., Carbonari, S., Dezi, F., Gara, F., & Leoni, G. (2021). A probabilistic investigation on the dynamic behaviour of pile foundations in homogeneous soils. Bulletin of Earthquake Engineering, 1-29.
[33] J. Jonkman, W. Musial, Offshore Code Comparison Collaboration (OC3) for IEA Task 23 Offshore Wind Technology and Deployment, techreport NREL/TP-5000-48191, National Renewable Energy Laboratory, 2010.
[34] P. Bartolotti, H. Canet Tarres, K. Dykes, K. Merz, L. Sethuraman, D. Verelst, F. Zahle, IEA Wind Task 37 on Systems Engineering in Wind Energy – WP2.1 Reference Wind Turbines, resreport NREL/TP-73492, International Energy Agency, 2019. https://github.com/IEAWindTask37/IEA-10.0-198-RWT.
[35] E. Gaertner, J. Rinker, L. Sethuraman, F. Zahle, B. Anderson, G. Barter, N. Abbas, F. Meng, P. Bartolotti, W. Skrzypinski, G. Scott, R. Fel, H. Bredmose, K. Dykes, M. Sheilds, C. Allen, A. Viselli, Definition of the IEA 15 MW Offshore Reference Wind Turbine, techreport NREL/TP-75698, International Energy Agency, 2020. https://github.com/IEAWindTask37/IEA-15-240-RWT.
[36] Ambraseys, N., Smit, P., Sigbjornsson, R., Suhadolc, P. and Margaris, B. (2002), Internet-Site for European Strong-Motion Data, European Commission, Research-Directorate General, Environment and Climate Programme.
[37] G.M. Álamo, J.D.R. Bordón, and J.J. Aznárez. On the application of the beam model for linear dynamic analysis of pile and suction caisson foundations for offshore wind turbines. Computers and Geotechnics, 134, 2021.
[38] Bucalem, M.L. &. Bathe, K.J. (1993). Higher-order MITC general shell elements. International Journal for Numerical Methods in Engineering, 36:3729–3754.
[39] Pak, R.Y.S. & Guzina B.B. (2002). Three-dimensional Green's functions for a multilayered half-space in displacement potentials. Journal of Engineering Mechanics, 128(4):449–461.
[40] Oñate, E. (2013). Structural Analysis with the Finite Element Method. Linear Statics. Volume 2. Springer
[41] Domínguez, J. (1993). Boundary Elements in Dynamics. WIT Press.
[42] Anoyatis, G. & Lemnitzer, A. (2017). Dynamic pile impedances for laterally–loaded piles using improved Tajimi and Winkler formulations. Soil Dynamics and Earthquake Engineering, 92:279-297.
[43] Novak, M., Aboul-Ella, F. & Nogami T. (1978). Dynamic soil reactions for plane strain case. Journal of the Engineering Mechanics Division, 104(4):953–959.
[44] Álamo,G.M, Bordón, J.D.R., Aznárez, J.J. & Maeso, O. (2018). Relevance of soil-pile tangential tractions for the estimation of kinematic seismic forces: Formulation and setting of a Winkler approach. Appl Math Model, 59:1–19.
[45] Novak, M. and Sheta M. (1982). Dynamic response of piles and pile groups. In proceedings on the 2nd International Conference of numerical methods in offshore piling. Austin, Texas; April 29-30.